DESIGN OF A MICROWAVE SYSTEM FOR MEASURING DARK AND PHOTO-CONDUCTIVITY OF SEMICONDUCTORS

Rakshita Ravi

Bachelor of Engineering
Electronic Engineering Major

Department of Electronic Engineering
Macquarie University

November 6, 2017

Supervisor: Dr Nikos Kopidakis

ACKNOWLEDGMENTS

I would like to acknowledge my supervisor, Dr Nikos Kopidakis for the continuous encouragement and support he has provided throughout my thesis project. I would like to express my gratitude to my co-supervisor Dr. Raheel Hashmi and tutor, Affan Baba, for their assistance in using CST Microwave Studio.

STATEMENT OF CANDIDATE

I, Rakshita Ravi, declare that this report, submitted as part of the requirement for the award of Bachelor of Engineering in the Department of Electronic Engineering, Macquarie University, is entirely my own work unless otherwise referenced or acknowledged. This document has not been submitted for qualification or assessment an any academic institution.

Student's Name: Rakshita Ravi

Student's Signature: Rakshita Ravi

Date: 06-11-2017

ABSTRACT

Semiconductor industry is evolving with new emerging semiconductor materials. Researchers and engineers constantly test and analyse these new materials for their conductivity to further develop this technology. The most traditional method of testing these have been through soldering electrical contacts onto the material. However, this is time consuming. Microwave probe technique used in this thesis is robust and uses relatively easy setup to analyse electronic properties of the samples. The semiconductor materials are simulated in rectangular open waveguide and cavity resonator. Different samples with varying conductivity, dielectric constant and sample thickness are probed to measure microwave absorption. Real photovoltaic samples, OPV, Silicon, Cadmium Telluride (CdTe) and Gallium Arsenide (GaAs) are simulated for their dark and photoconductivity by changing their doping. For dark conductivity simulations, GaAs has the highest conductivity and power absorption of 23 % and OPV has the lowest conductivity and power absorption of 1.5 % for low doping. For photoconductivity simulations, proposed cavity model worked only for low conductivity samples such as OPV, and it has the capacity to absorb maximum power of 6%. Silicon, CdTe and GaAs were simulated in open waveguide as they were shorting the cavity due to high reflection. GaAs absorbs maximum power of 35 %, silicon absorbs 14 % and CdTe absorbs 9%. These results indicate that the proposed design is suitable for probing low conductivity semiconductor materials.

Contents

List of Figures

List of Tables

Chapter 1

Introduction

Semiconductors dominate the modern-day electronics, they are an essential substance in electronic devices such as solar cells, LEDs, mobile phones, computers, and more. The unique atomic structure of the semiconductor allows the conductivity to be easily controlled. Conductivity is an intrinsic property of semiconductor and it depends on the resistivity of the material.

The sheer popularity and high demand of semiconductors in modern world has led to new organic and inorganic semiconductor materials to emerge in this industry. This has led to the requirement of a reliable and efficient testing technique to probe these new materials for their electronic properties. This will assist in future development of semiconductor technology. Semiconductor materials have been tested previously by others using various methods. The most popular method has been through soldering metal electrical contacts onto the material. The main disadvantage of using this method is that it is time consuming and requires personnel with good skill.

This thesis uses an alternative method which is relatively easy and robust to test conductivity in semiconductors. This is achieved through Time Resolved Microwave Conductivity (TRMC). TRMC is a contactless conductivity probing technique, which involves measuring the transmission of microwave signal through the sample as a function of time after the pulse has hit the sample.

Simulations will be conducted using computer simulation technology (CST) and the results obtained from these simulations are valuable and play a significant role in prototyping. In the actual experimental setup (prototype), the only results TRMC can provide are quantitative results such as the amount of power absorbed, reflected and transmitted by the sample and then these results are used to translate it to the samples electronic properties. The simulation results obtained in this thesis provides quantitative results as well as qualitative results. For instance, qualitative results provide a greater understanding of how the electrical and magnetic fields interact with the sample. There are numerous books that has mathematical analysis on these topics and some field maps. The simulation results in this thesis shows the field interaction with open waveguide, cavity, quartz and different samples. Qualitative illustrations such as these field maps provide clear visualisation which makes it easier to comprehend the underlying principles. These

simulation results assist in designing the experiment in a better way. This technique has been used previously by others to test low conductivity samples. This thesis investigates if the proposed design is suitable to measure both low conductivity and high conductivity samples, if it can probe materials of interest to solar industry.

The layout of this thesis is such that Chapter 2 contains the background information relevant to this thesis. In particular, it covers the basic concepts on TRMC technique, Rectangular waveguide, S parameters and CST Microwave Studio. Chapter 3 looks at semiconductor materials in an open waveguide. It talks about different waveguide configurations and the simulation results of quartz and sample materials in terms of power transmission, absorption and reflection in open waveguide. Chapter 4 looks at semiconductor materials in cavity resonator which is designed from WR90 open waveguide from chapter 3. Chapter 4 contains simulation results of sample materials and real photovoltaic materials such as, OPV, Silicon, Cadmium Telluride and Gallium Arsenide in the cavity. Chapter 5 looks at photoconductivity of the materials discussed in chapter 4 and investigates how flashing light onto the semiconductor can impact their power absorption of microwaves.

Chapter 2

Background

2.1 What is TRMC?

The underlying principle behind Flash Photolysis Time Resolved Microwave Technique (FP-TRMC) is the microwave absorption by free electrons. In FP-TRMC, the sample is placed inside a cavity resonator at position of maximum electric field strength such that when microwaves is applied to the sample, and the light is flashed onto the material, the photo induced carriers within the sample are excited and absorbs particular range of frequencies. When the light is turned-off, then the carriers return to their stable state, restoring the microwave intensity. This process is better illustrated in Figure 2.1. In Figure 2.1 A, microwaves (probe) is applied to the sample. Figure 2.1 B, Light is flashed onto the sample, and the carrier charges are exited. Microwave intensity is reduced while leaving the sample. Figure 2.1 C, Light is turned-off, the carrier charges are returning back to their normal state (very few mobile charges present), and microwave intensity is restored. [1] [2]

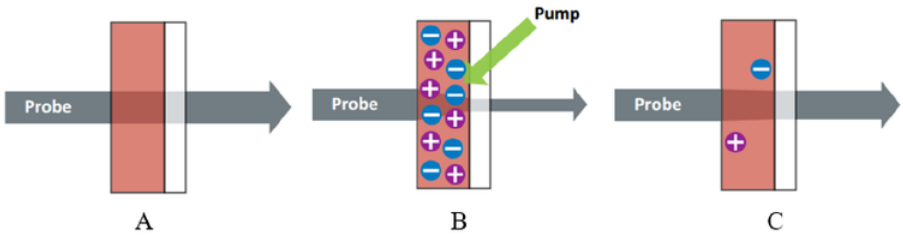

Figure 2.1: Absorption and Restoration of Microwaves in FP-TRMC. [2]

The restoration of microwave takes place over a certain period of time. The absorption and the restoration of the waves indicate a lot about the properties of the material and in particular about its conductivity. In simple terms, and to a certain extent, the change in absorbed microwave power is proportional to the change in conductivity of the sample.

TRMC technique was first used by Margenau in mid-40s to analyze the behavior of charged particles in their gaseous form. This became popular after Warman and De Haas introduced PR-TRMC technique and then later evolved to FP-TRMC (Flash Photolysis Time Resolved Microwave Conductivity) in early 80s, where laser light was used as the radiation source. A qualitative illustration of TRMC technique setup used by others is shown in Figure 2.2. The sinusoidal lines in the figure represent the standing-wave pattern of the microwave electric fields. Notice, sample is placed at a position where there is maximum electric field strength inside the cavity. A better understanding of these electric fields and their interaction with sample can be gained by the simulation results in the following chapters.

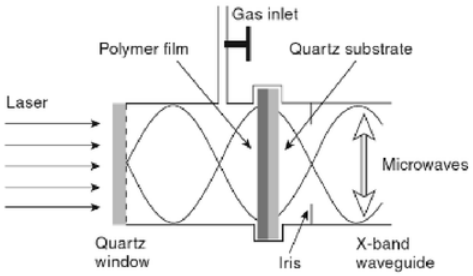

Figure 2.2: Schematic of TRMC technique setup using microwave cavity resonator and sample. [3]

The main advantage of using FP-TRMC technique is that, it is guaranteed that the number of mobile electrons created in the semiconductors conduction band is related to its change in conductivity. FP-TRMC can be used to monitor the generation of charge carriers in thin films and in particular it is very useful in determining the key parameters of the photoactive part of the photovoltaic device. [4]

2.2 Rectangular Waveguide

Rectangular waveguides are one of the earliest and well known technology used to transport microwave signals with their frequency band ranging from 1 GHz to over 220 GHz. Waveguides have certain boundary conditions that restrict the propagation mode.

- The electric field must be orthogonal to the conductor in order to exist at the surface of that conductor.
- The magnetic field must not be orthogonal to the surface of the waveguide.

Due to these boundary conditions, waveguides have transverse electric (TE) and transverse magnetic (TM) modes for propagation. Transverse electric (TE) and Transverse

magnetic (TM) have different field configurations. A simple notation can be used to describe various modes of propagation as shown below:

$$Tx_{m,n} \tag{1}$$

where

x = E for transverse electric mode, and M refers to transverse magnetic mode

m = the number of half-wavelengths along the x axis

n = the number of half-wavelengths along the y axis

TE wave has E_x, E_y, H_x, H_y, and H_z components. TM wave has E_x, E_y, E_z, H_x and H_y components. Signal propagation in a waveguide depends on the frequency of the input signal. EM waves propagate inside the waveguide only when the frequency of the applied signal is higher than the cut-off frequency $f_{c,mn}$. [5] [6]

$$f_{c,mn} = \frac{1}{2\pi\sqrt{\mu\epsilon}}\sqrt{(\frac{m\pi}{a})^2(\frac{n\pi}{b})^2} \qquad m, n = 0, 1, 2, ... \tag{2}$$

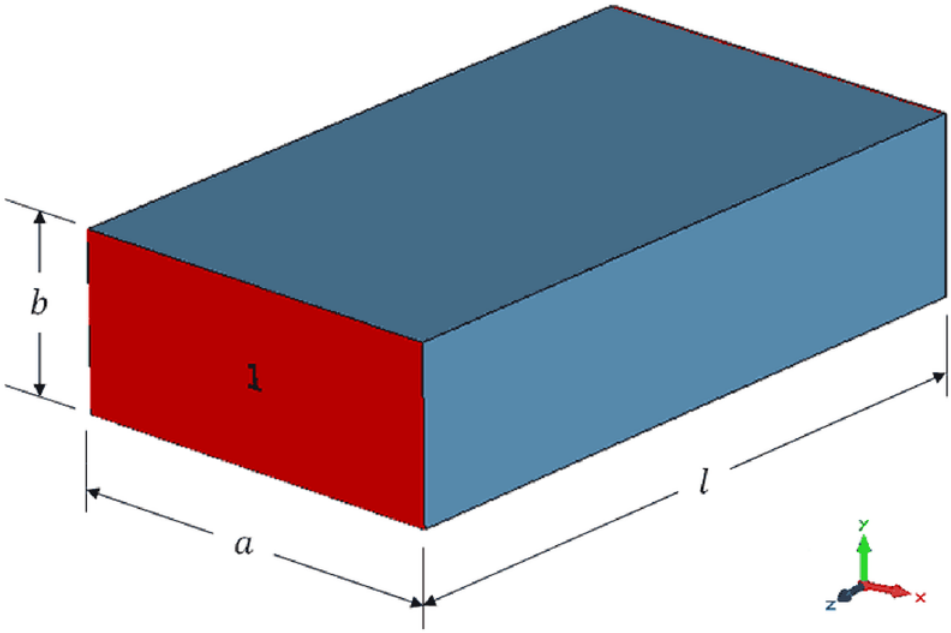

Figure 2.3: Schematic of rectangular waveguide with axes and dimensions. [7]

WR90 is metallic X band rectangular waveguide and its cross-sectional dimensions are a=22.86 mm and b=10.16 mm. Figure 2.3 shows the schematic of the rectangular waveguide with dimensions a and b labelled. X-band region has frequencies from 8 GHz to

Table 2.1: $TE_{m,n}$ mode cutoff frequencies

m	n	$f_{c,mn}$GHz
1	0	6.562
2	0	13.123
0	1	14.764
1	1	16.156

Table 2.2: $TM_{m,n}$ mode cutoff frequencies

m	n	$f_{c,mn}$ GHz
1	1	16.156
1	2	30.248
2	1	19.753

12.5 GHz and the Tables 2.1 and 2.2 indicate that WR90 allows TE10 mode to propagate in the waveguide and this is also the dominant mode.

2.3 S Parameters

Scattering parameters or S parameters define the input output relationship between the device ports.

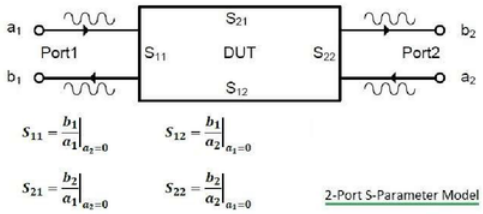

Figure 2.4: Schematic of 2-port S-parameter model. [8]

Applying the figure 2.4 to this thesis, the source is on Port 1 and detection is on Port 2. This way a_1 is the incident power, b_1 is the reflected power, b_2 is the transmitted power and a_2 on the Port 2 will be eliminated (i.e. $a_2 = 0$). This eliminates the S_{12} and S_{22} parameters leaving behind just S_{11} and S_{21}. Now S_{11} can be considered as the input reflection coefficient and S_{21} as transmission coefficient. [9] [10]

The equations below represent S_{11} and S_{21} in terms of incident field (E_i), reflected field (E_r) and transmitted field (E_t). All S parameter equations mentioned below are in dB scale.

$$S_{11} = 20log_{10}\left|\frac{E_r}{E_i}\right| \tag{3}$$

$$S_{21} = 20log_{10}\left|\frac{E_t}{E_i}\right| \tag{4}$$

2.3.1 Return Loss and Insertion Loss

Return loss (RL) is a measure of effectiveness of delivering power from source (Port 1) to load. RL is the difference in dB between input power (P_I), and reflected power (P_R). Insertion Loss is the loss of signal power during signal transmission and similar to RL, IL is a positive quantity. The below equations represent RL and IL in terms of input power (P_I), reflected power (P_R) and transmitted power (P_T). [11]

$$RL = 10log_{10}\left(\frac{P_I}{P_R}\right) \tag{5}$$

$$IL = 10log_{10}\left(\frac{P_I}{P_T}\right) \tag{6}$$

RL and S_{11} can be easily converted to one another. This relationship holds between IL and S_{21}. [12]

$$S_{11} = 20log_{10}\left|\frac{E_r}{E_i}\right| dB = 10log_{10}\left|\frac{E_r}{E_i}\right|^2 dB = 10log_{10}\left(\frac{P_R}{P_I}\right) \tag{7}$$

Therefore, RL dB = -S_{11} dB and IL dB = -S_{21} dB

$$S_{11} = 10log_{10}\left(\frac{P_R}{P_I}\right) \tag{8}$$

$$S_{21} = 10log_{10}\left(\frac{P_T}{P_I}\right) \tag{9}$$

2.4 CST Microwave Studio

CST Studio Suite is a simulation platform for electromagnetic (EM) field problems and related applications. They currently offer seven modules namely, CST Microwave Studio, CST EM Studio, CST Particle Studio, CST Design Studio, CST PCB Studio, CST Cable Studio and CST MPhysics Studio. This thesis uses CST Microwave Studio which is used for EM design, simulation and analysis of high frequency problems. This studio is capable of analysing components such as single and multi-element antennas, filters, waveguides, resonators and many more. This module offers a range of solvers that can be used depending on the application and hence, this studio can solve basically any high frequency field problem. In this thesis, the experimental setup is quite simple with basic

structure and time and frequency domain solver is sufficient to simulate this structure. Time domain and frequency domain solver relies on Maxwells equations when simulating the structure and it provides simulation results which are extremely useful when studying the field propagation through a component. [13]

Chapter 3

Semiconductor materials in Open Waveguide

Rectangular Waveguide modelled in CST is a replicate of WR90 waveguide available in store. Before directly testing the semiconductor samples, initial testing was performed on just waveguides. This was done to check the effectiveness of microwave propagation within the waveguide. Numerous experimental setups and model configurations were investigated to find the best suitable configuration which would deliver the most reliable, accurate and desirable results. Much time was dedicated for these initial stages because it is crucial to get them right as the later stages of this thesis are heavily dependent on these experimental setup.

3.1 Open Waveguide Configurations

A number of factors can affect the microwave propagation within the waveguide, however the major factors include the material of the waveguide, length of the waveguide, and the wall thickness of the waveguide.

3.1.1 Material and Length of the waveguide

Waveguide model specifications

- Inner Dimensions: a = 22.86 mm, b = 10.16 mm
- Length of the waveguide (z axis): 50 mm, 100 mm and 150 mm
- Number of ports: 2
- Wall thickness: 0.5 mm
- Material of the waveguide: Brass (91%) and Silver.
- Material inside the waveguide: Vacuum

- Input Power (P_I) = 0.5W

Metals have low resistivity which is a key factor because lower resistivity increases the efficiency of microwave power transmission. Hence, most of the waveguides are made from metals such as brass, silver, aluminium, gold, etc. This section looks at brass and silver waveguides. Figure 3.1 displays the models of brass and silver waveguides along with their material configurations. These models are simulated using T solver and hexahedral mesh type. T solver provides numerous 1D, 2D/3D results, however the results that are of interest for this thesis are the E-field and H-field distribution, and S-parameters.

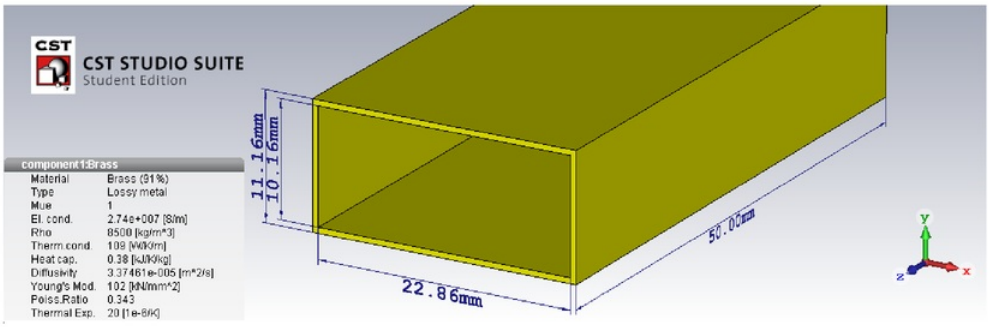

(a) Brass Waveguide

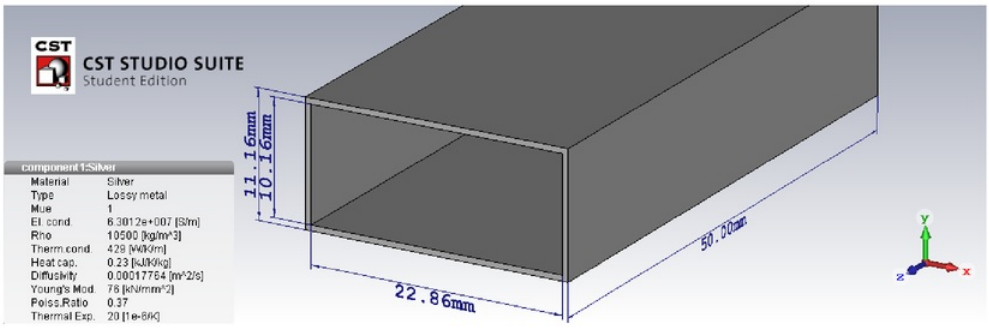

(b) Silver Waveguide

Figure 3.1: Hollow waveguide model

Field Distributions

The E-field and H-field distribution in figure 3.2 are obtained from brass model in figure 3.1a. These field distributions indicate that waveguide is in TE_{10} mode and these results support the concept discussed in background chapter.

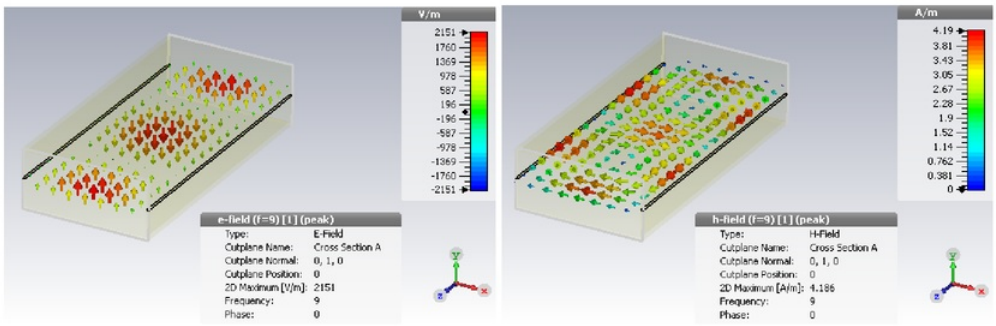

(a) E-field cross-section 1

(b) H-field cross-section 1

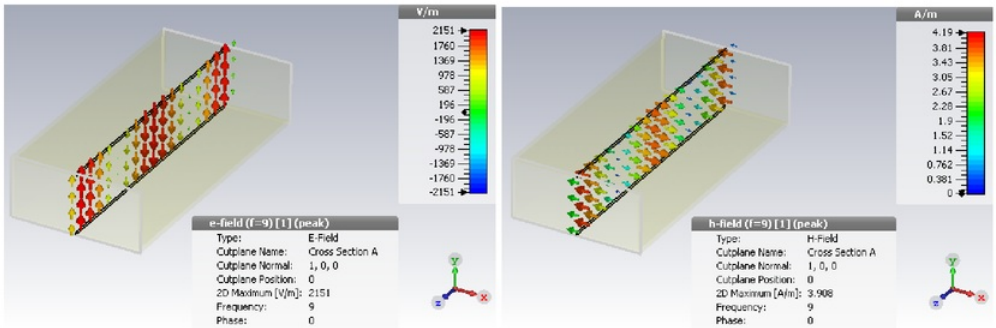

(c) E-field cross-section 2

(d) H-field cross-section 2

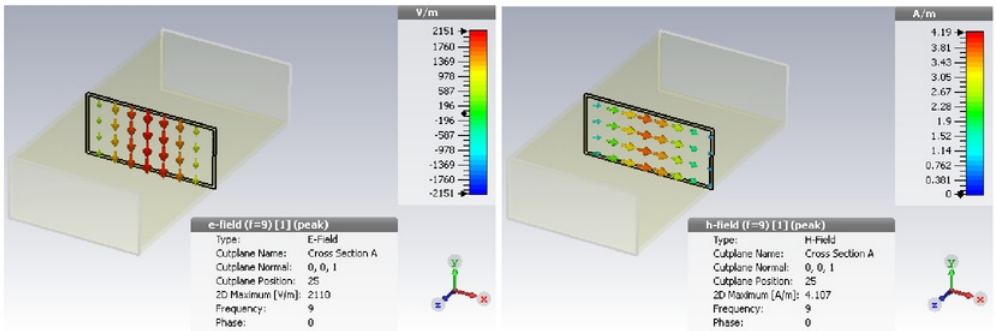

(e) E-field cross-section 3

(f) H-field cross-section 3

Figure 3.2: TE_{10} Field Distribution

S Parameters

S parameters (S_{11} and S_{21}) values obtained from each waveguide can be used to calculate reflected power P_R and transmitted power P_T. This is achieved by rearranging the equations (8), (9) to obtain equation (10), (11). P_L in equation 12 represents power loss in the waveguide and P_I represents input power. Table 3.1 and 3.2 are derived by substituting S-parameters at 9 GHz into equation (10) - (12).

$$P_R = 10^{(\frac{S11}{10})} \times P_I \tag{10}$$

$$P_T = 10^{(\frac{S21}{10})} \times P_I \tag{11}$$

$$P_L = P_I - (P_R + P_T) \tag{12}$$

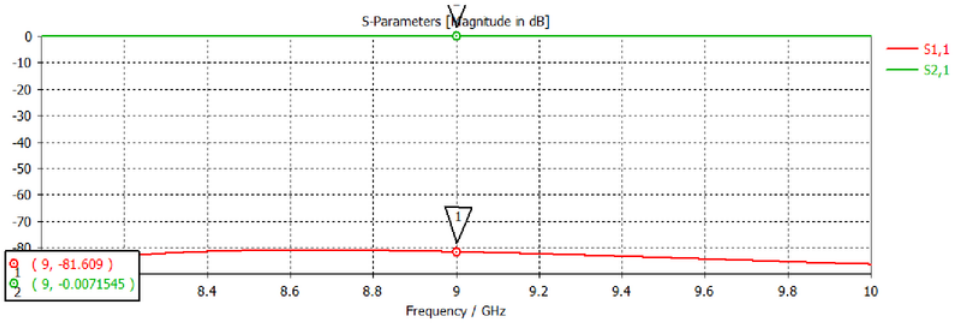

Figure 3.3: S-Parameters graph from 50 mm brass waveguide

Table 3.1: Brass Hollow Waveguide

Length(mm)	S_{11}(dB)	S_{21}(dB)	P_R (W)	P_T (W)	P_T %	P_R %	P_L
50	-81.609	-0.007	3.45E-09	0.499	99.83	6.9E-07	0.0008
100	-80.987	-0.017	3.98E-09	0.498	99.6	7.9E-07	0.0019
150	-81.106	-0.033	3.87E-09	0.496	99.2	7.7E-07	0.0038

Table 3.2: Silver Hollow Waveguide

Length(mm)	S_{11}(dB)	S_{21}(dB)	P_R (W)	P_T (W)	P_T %	P_R %	P_L
50	-85.229	-0.004	1.49E-09	0.499	99.89	2.9E-07	0.0005
100	-84.596	-0.011	1.73E-09	0.498	99.7	3.4E-07	0.0013
150	-84.706	-0.024	1.69E-09	0.497	99.4	3.38E-07	0.0027

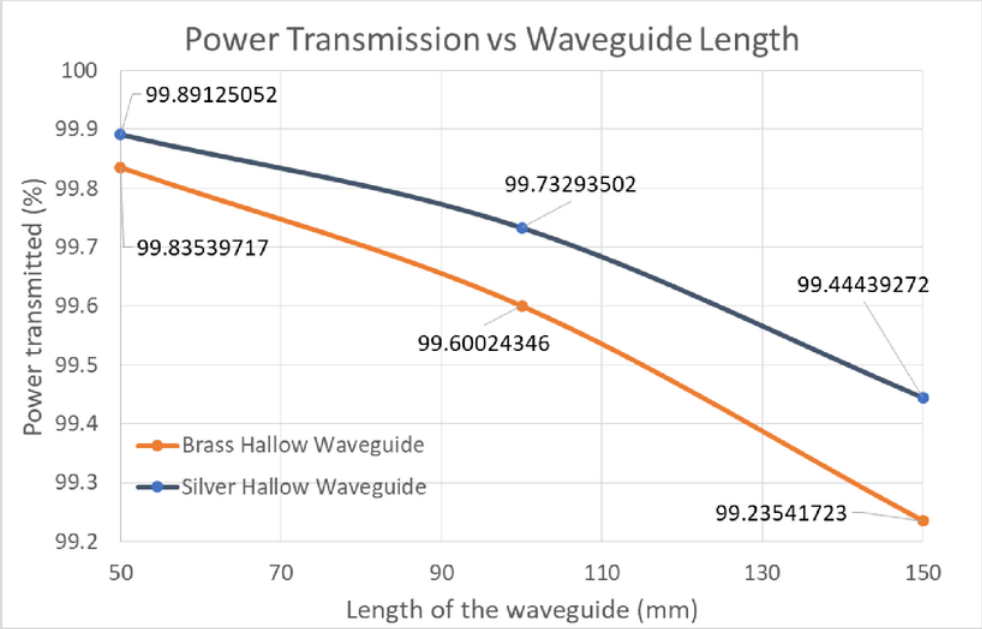

Figure 3.4: Power Transmission in Brass and Silver waveguide with varying lengths

Waveguides are predominately made from brass as it is relatively cheap, but waveguides also come with silver plating which reduces the resistance loss and increases the waveguide efficiency. However, waveguides with silver plating is expensive. The results from figure 3.4 indicates that silver is slightly better than brass waveguide. The difference between silver and brass power transmission is less than 0.2% and upgrading a brass waveguide to a silver plated waveguide is not worth it for such small difference.

The figure 3.4 also indicates that the percentage of power transmission is reduced as the length of the waveguide is increased. Since neither brass or silver are perfect metals, instead they are lossy metals and the waveguide is not infinitely long, this results in power losses and reflection during microwave propagation. At this stage, a 100 mm brass waveguide will be suitable for this thesis.

3.1.2 Waveguide wall thickness

Wall thickness of the waveguide depends on the skin depth of the material. The skin depth of brass material at 9 GHz frequency is as following

$$\delta_S = \sqrt{\frac{2}{\omega\mu\sigma}} = \sqrt{\frac{1}{\pi f \mu_o \sigma}} \tag{13}$$

Where:

μ_o = Permeability = $4\pi \times 10^{-7}$
σ = Conductivity of metal (Brass) = 2.56×10^7
f = 9 GHz
Therefore, from equation (13), $\delta_S = 1\mu m$

Waveguide model specifications

- Inner Dimensions: a = 22.86 mm, b = 10.16 mm
- Length of the waveguide (z axis): 100 mm
- Wall thickness: 0.5 mm, 1 mm and 1.5 mm
- Material of the waveguide: Brass (91%)
- Material inside the waveguide: Vacuum
- Input Power (P_I) = 0.5 W

Table 3.3: Brass Open Waveguide with different wall thickness

Wall Thickness(mm)	S_{11}(dB)	S_{21}(dB)	P_R (W)	P_T (W)	P_T %	P_R %	P_L %
0.5	-80.99	-0.017	3.98E-09	0.498	99.6	7.96E-07	0.002
1	-80.95	-0.017	4.01E-09	0.498	99.6	8.03E-07	0.002
1.5	-80.95	-0.018	4.02E-09	0.498	99.6	8.03E-07	0.002

Figure 3.5 indicates that P_T remains at 99.6 % for wall thickness between 0.5 mm and 1.5 mm. This less than 1 % of power loss is due to brass not being a perfect metal and the waveguide walls are not infinitely thick.

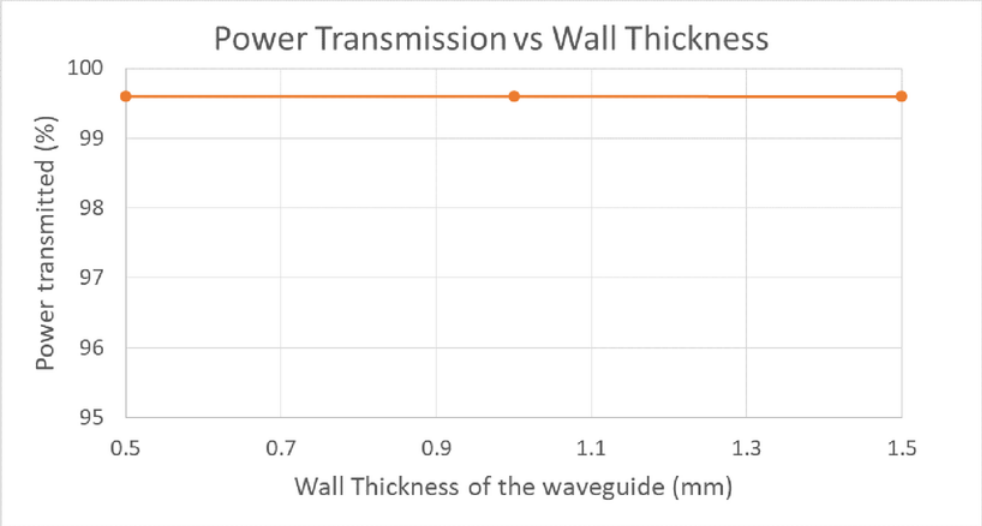

Figure 3.5: Power Transmission in Brass waveguide with varying wall thickness

3.2 Open Waveguide with Quartz

Quartz plays an important role throughout this thesis even though it is not an object of interest. Some semiconductor materials such as OPV, need to be deposited on a piece of quartz before placing it in the waveguide or cavity. To keep the experiment controlled, quartz is tested and analyzed for its microwave absorption before depositing semiconductor materials on it. This helps in differentiating the amount of microwaves absorbed by the quartz and by the semiconductor material at the final stage. Figure 3.6 shows 100 mm brass waveguide model with quartz at 50 mm (i.e. half way through the waveguide).

Power absorption can be found by subtracting the power loss of hollow waveguide $\left(P_L \text{ (hollow)}\right)$ from power loss of waveguide with quartz $\left(P_L \text{ (quartz)}\right)$ and this can be seen in equation (14)

$$P_A(quartz) = P_L(quartz) - P_L(hollow) \tag{14}$$

Waveguide model specifications

- Inner Dimensions: a = 22.86 mm, b = 10.16 mm
- Length of the waveguide (z axis): 100 mm
- Wall thickness: 0.5 mm
- Material of the waveguide: Brass (91%) lossy metal

- Material inside the waveguide: Vacuum
- Input Power (P_I) = 0.5 W

Quartz specifications

- Inner Dimensions: a = 22.86 mm, b = 10.16 mm
- Quartz thickness: 1 mm
- Quartz placement (on z axis): 50 mm
- Material: Quartz (lossy)

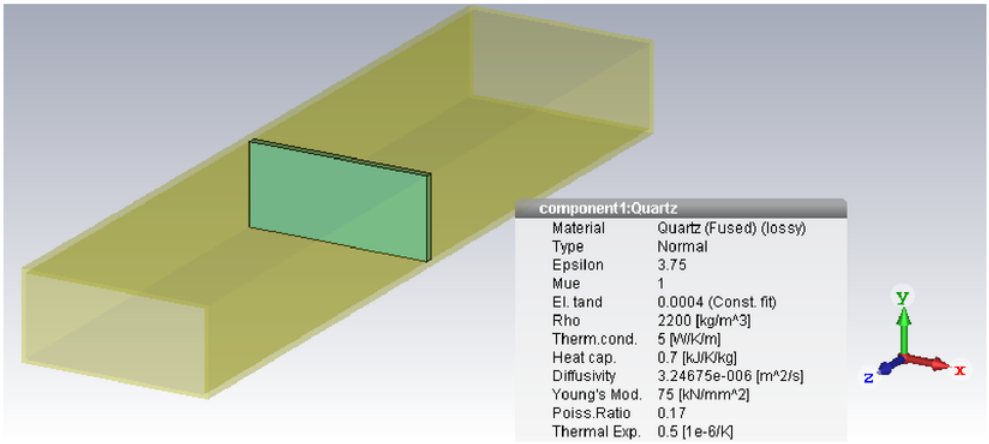

Figure 3.6: Brass waveguide with quartz placed at 50 mm on z axis

Field Distributions

Figure 3.7 shows the field distributions for open waveguide model with and without quartz. In these models, the quartz is placed in the middle of the waveguide and the effect quartz has on field distribution is clearly visible and highlighted in figures 3.7 a and b. Notice, E-field and H-field are higher for quartz on input side (Port 1) as opposed to hollow waveguides. This is due to the reflected waves from quartz being in phase with the incident waves which causes the resulting fields to be amplified near port 1.

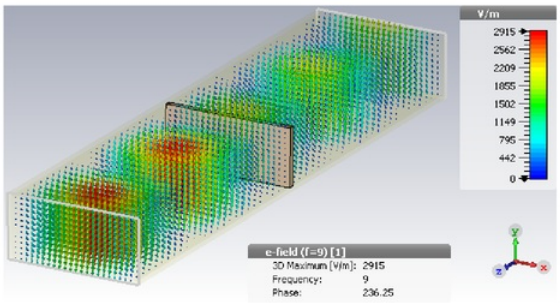

(a) E-field with quartz

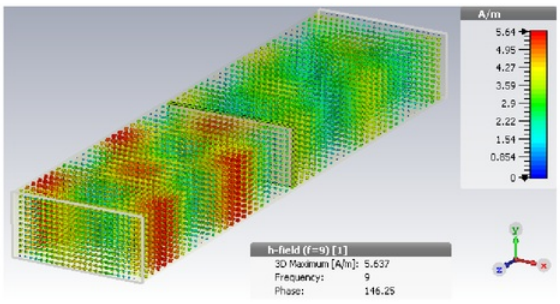

(b) H-field with quartz

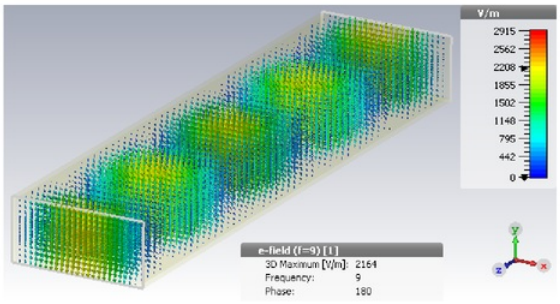

(c) E-field without quartz

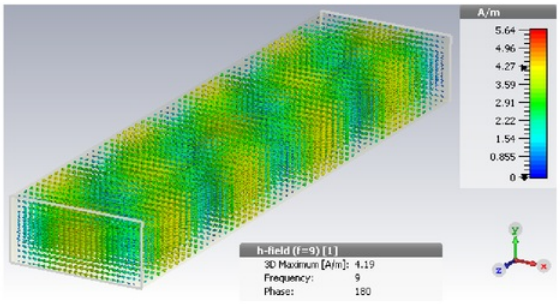

(d) H-field without quartz

Figure 3.7: Effect of Quartz on Field Distribution

S Parameters

Until now, there was only one material inside the hollow waveguide, which was vacuum. But now, microwaves have to travel through vacuum as well as quartz which are two very different medium and have different refractive index. The change in medium causes the microwaves to be reflected, absorbed and transmitted. The amount of power transmitted, reflected and absorbed can be seen in figures 3.8 to 3.10.

The presence of quartz has a great impact on power transmission and reflection as shown in figure 3.8 and 3.9. Quartz increases the power reflection by 12% as compared to power reflection in hollow waveguide. Power loss due to imperfections in open waveguide is the major contributor to the difference between power transmission and power reflection rather than the presence of quartz in the open waveguide. Figure 3.10 indicates that absorption in quartz is extremely low.

Table 3.4: Brass Waveguide with Quartz

Length(mm)	S11(dB)	S21(dB)	P_R (W)	P_T (W)	P_L (W)	P_A (W)
50	-9.1623	-0.57	0.0606	0.438	0.001	0.000179
100	-9.1488	-0.58	0.0608	0.436	0.002	0.000178
150	-9.1563	-0.60	0.0607	0.435	0.004	0.000331

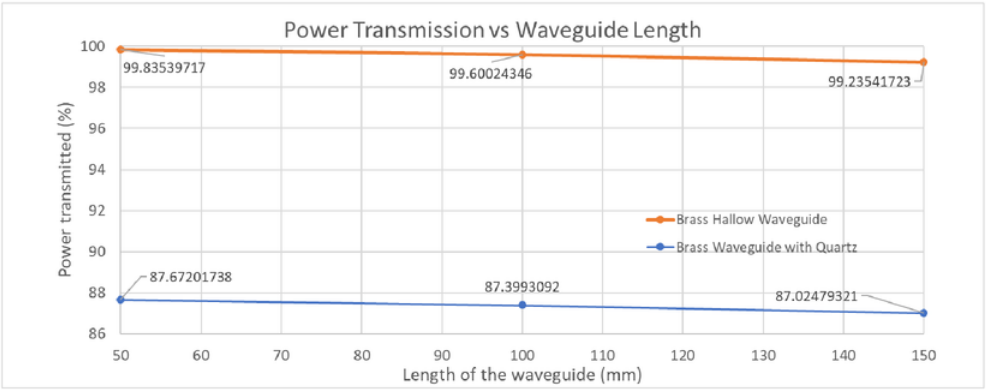

Figure 3.8: Power Transmission in Brass waveguide with and without quartz

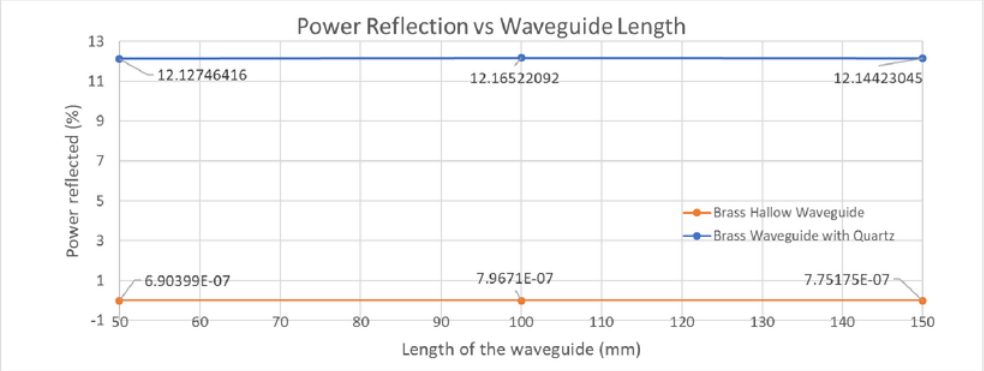

Figure 3.9: Power Reflection in Brass waveguide with and without quartz

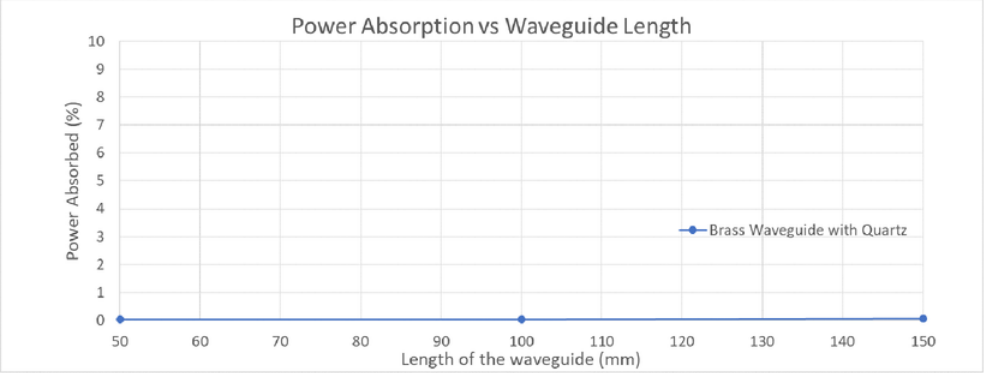

Figure 3.10: Power Absorption by quartz in brass waveguide

3.2.1 Quartz placement

Position of quartz within the waveguide is one of the factors that needs to be investigated. Power transmission, absorption and reflection was investigated by varying the quartz position within the waveguide as shown in table 3.5.

Figure 3.11 to 3.13 indicate that position of the quartz in an open waveguide does not have a massive impact on power transmission, reflection or absorption as they are approximately 87.4%, 12.1% and 0% respectively.

Table 3.5: 100 mm Brass Waveguide with varying quartz position

Position(mm)	S11(dB)	S21(dB)	P_R (W)	P_T (W)	P_L (W)	P_A (W)
25	-9.145	-0.583	0.0608	0.437	0.0020	-0.0001
50	-9.148	-0.584	0.0608	0.436	0.0021	4.2E-10
75	-9.172	-0.583	0.0604	0.437	0.0024	0.00023

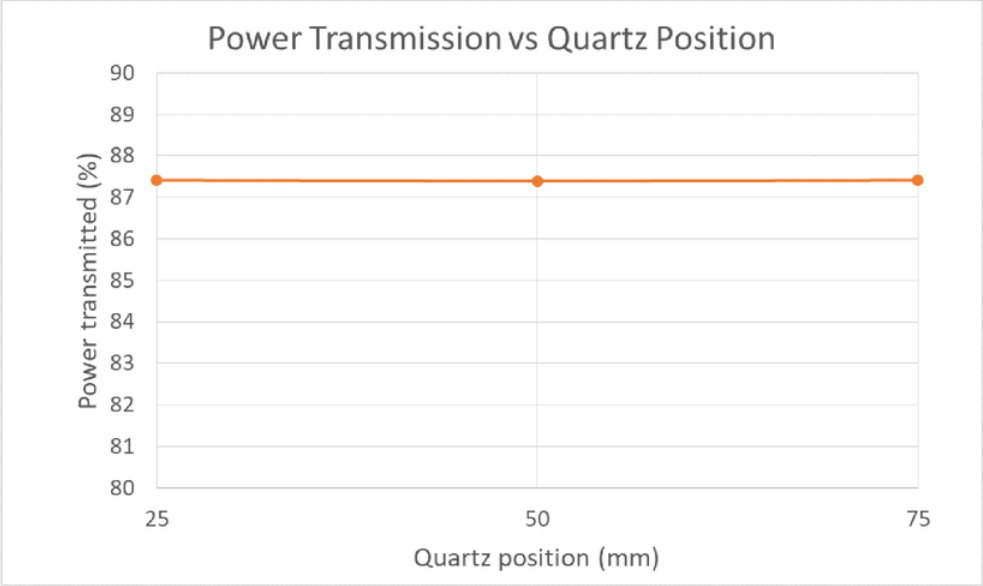

Figure 3.11: Power Transmission with different quartz position

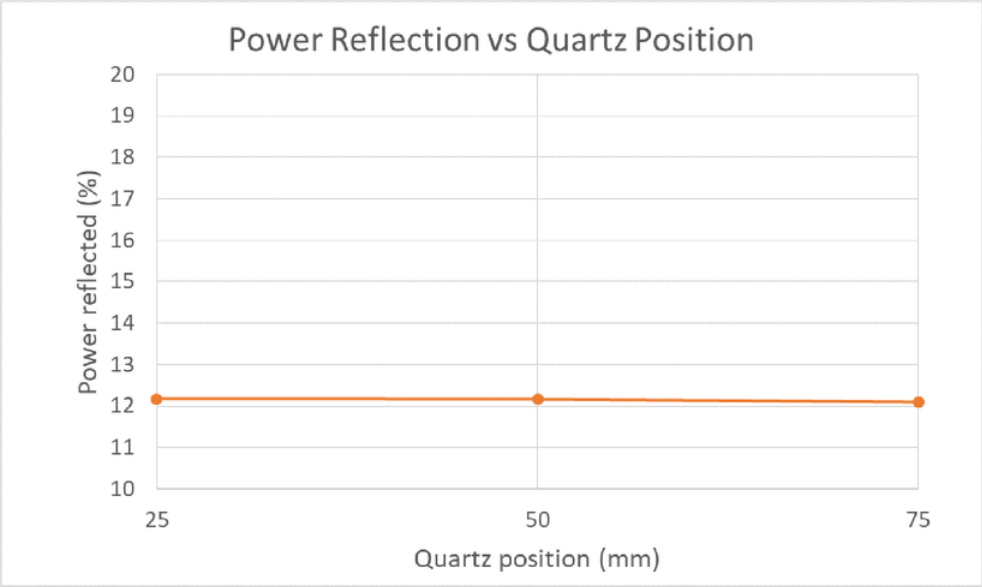

Figure 3.12: Power Reflection with different quartz position

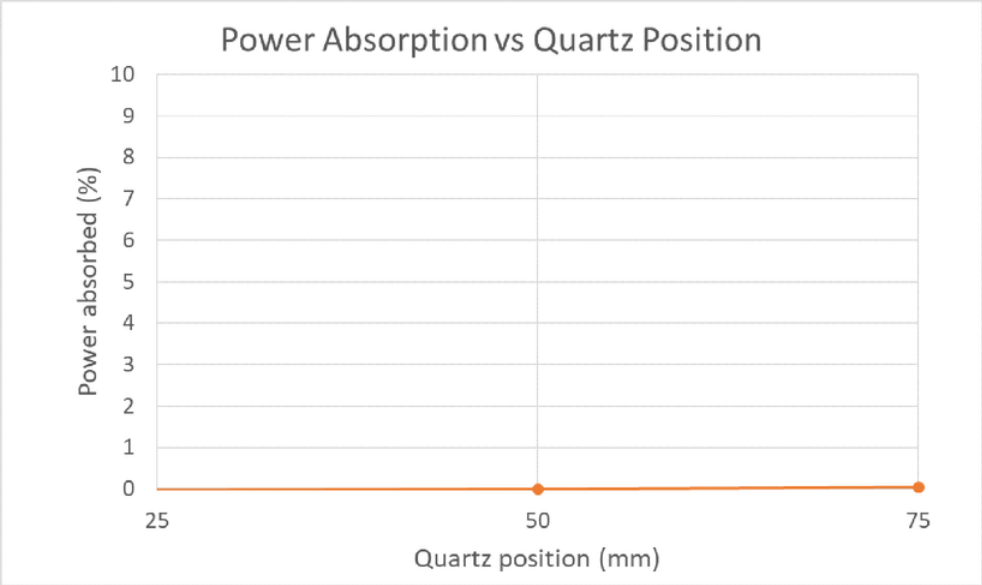

Figure 3.13: Power Absorption with different quartz position

3.3 Open Waveguide with Test Sample

In this section, test samples with different electrical properties are deposited on top of quartz and their P_T, P_R and P_A are analyzed. Figure 3.14 shows the open waveguide model where test sample (pink) is placed on top of quartz (green). Power reflected and absorbed by the sample can be calculated using the equations 15 and 16, where P_L (quartz) and P_R (quartz) values were found in section 3.2.

$$P_A(sample) = P_L(Total) - P_L(Quartz) \tag{15}$$

$$P_R(sample) = P_R(Total) - P_R(Quartz) \tag{16}$$

where:

- P_L (quartz) = 0.002177 W
- P_R (quartz) = 0.060826 W

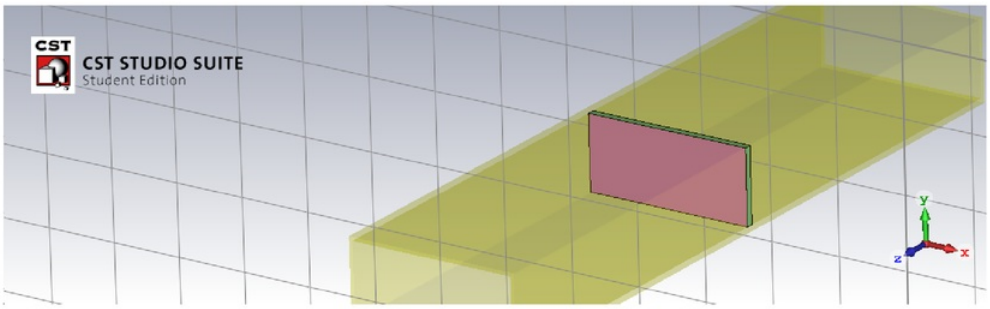

Figure 3.14: Open waveguide with test sample deposited on top on quartz

3.3.1 Test sample with different conductivity

Conductivity (σ) is a measure of material's ability to conduct electric current and is represented by reciprocal of electrical resistivity (ρ).

$$\sigma = \frac{1}{\rho} \tag{17}$$

Test Sample specifications

- Dielectric constant (ϵ): 3
- Test Sample thickness: 1 μm
- Conductivity (σ): 1.6×10^{-6} $\frac{S}{m}$, 1.6×10^{-3} $\frac{S}{m}$, 1.6 $\frac{S}{m}$

Power analysis

Conductivity of the material has big impact on microwave absorption because at higher conductivity, material has more number of free electron charges that can readily absorb or reflect microwaves. This relationship can be seen in figure 3.15, as the conductivity of the test sample is increased, the power absorbed by the test sample is also increased. Table 3.6 contains the results obtained with respect to change in conductivity of test the sample and P_A (sample) and P_R (sample) are calculated from equations 15 and 16.

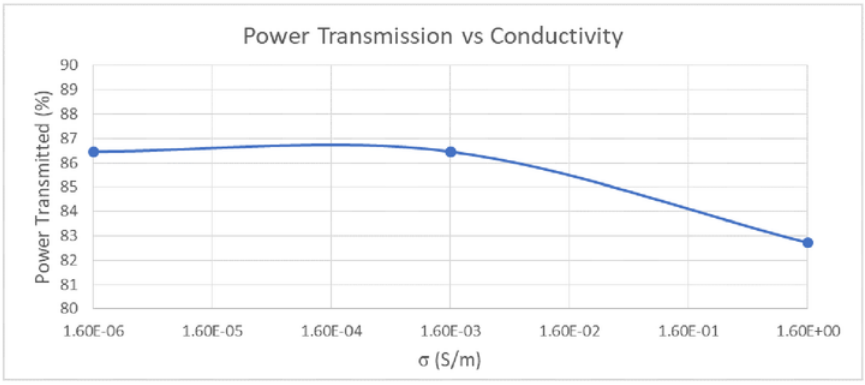

(a) Power Transmission in presence of test sample

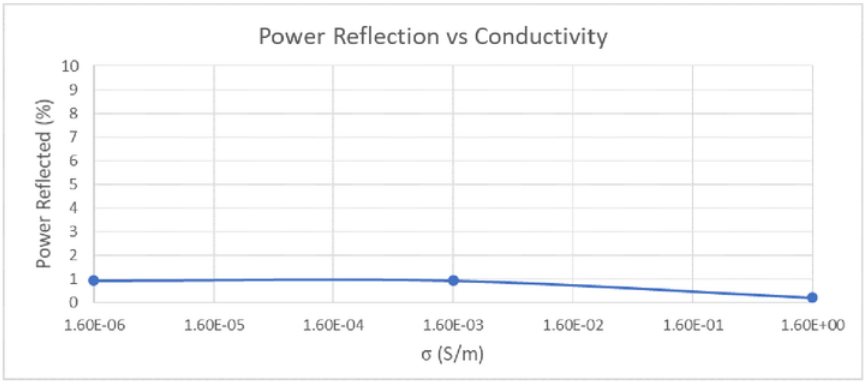

(b) Power Reflected by the test sample

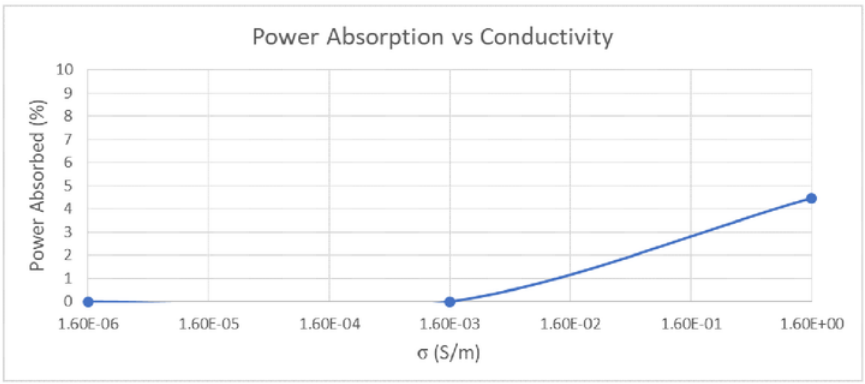

(c) Power Absorbed by the test sample

Figure 3.15: Power graphs for test sample with different conductivity

Table 3.6: Test sample of different conductivity in an open waveguide

σ ($\frac{S}{m}$)	S11(dB)	S21(dB)	$P_{R(total)}$ (W)	$P_{T(total)}$ (W)	$P_{L(total)}$ (W)	$P_{R(sample)}$ (W)	$P_{A(sample)}$ (W)
1.6×10^{-6}	-8.8277	-0.6315	0.06549	0.43233	0.00217	0.004	-1.7E-6
1.6×10^{-3}	-8.828	-0.6317	0.06548	0.43231	0.00219	0.004	2.16E-5
1.6	-9.0767	-0.8239	0.06184	0.41359	0.02455	0.001018	0.022

3.3.2 Test sample with different dielectric constant

Dielectric constant (ϵ) of the material represents the dipole moment or in particular the polarisation of the material. Therefore, dielectric constant can be defined as polarising the material which can absorb electric fields but it does not create conductivity. Material with high dielectric constant has higher polarisation ability and this factor plays an important role because if the material has high relative dielectric constant then it has low binding energy, i.e. they are easily polarised.

Test Sample specifications

- Dielectric constant (ϵ): 3, 5, 7
- Test Sample thickness: 1 μm
- Conductivity (σ): 1.6×10^{-3} $\frac{S}{m}$,

Power analysis

Figure 3.16 displays the power transmission, absorption and reflection of test sample with different dielectric constant. Regardless of change in dielectric constant, power absorbed by the test sample is approximately 0%. The power transmission and reflection graphs display a continuous trend as expected and the power reflection is increased as the dielectric of the sample is increased. This aligns with the theory that materials with high dielectric constant have high refractive index. High refractive index leads to increase in power reflection.

Table 3.7: Test sample of different conductivity in an open waveguide

ϵ	S11(dB)	S21(dB)	$P_{R(total)}$ (W)	$P_{T(total)}$ (W)	$P_{L(total)}$ (W)	$P_{R(sample)}$ (W)	$P_{A(sample)}$ (W)
3	-8.828	-0.6317	0.0654	0.4323	0.00219	0.0047	2.16E-5
5	-7.3955	-0.8971	0.0910	0.4067	0.0022	0.0302	5.66E-5
7	-6.6476	-1.0836	0.1081	0.3896	0.0022	0.0473	3.5E-5

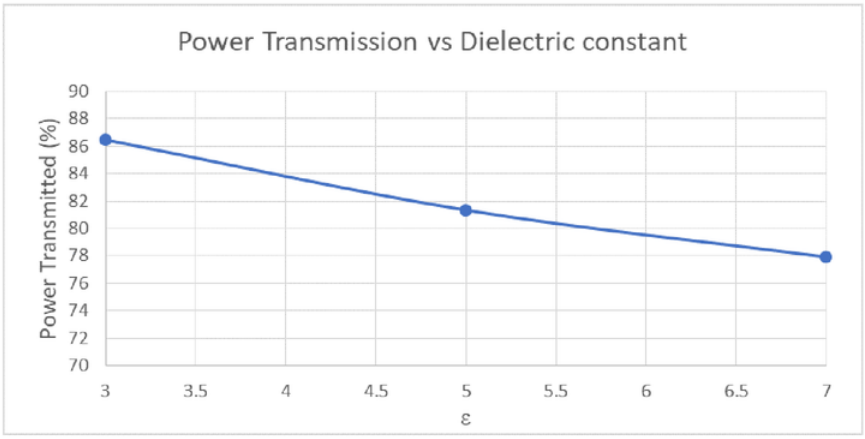

(a) Power Transmission in presence of test sample

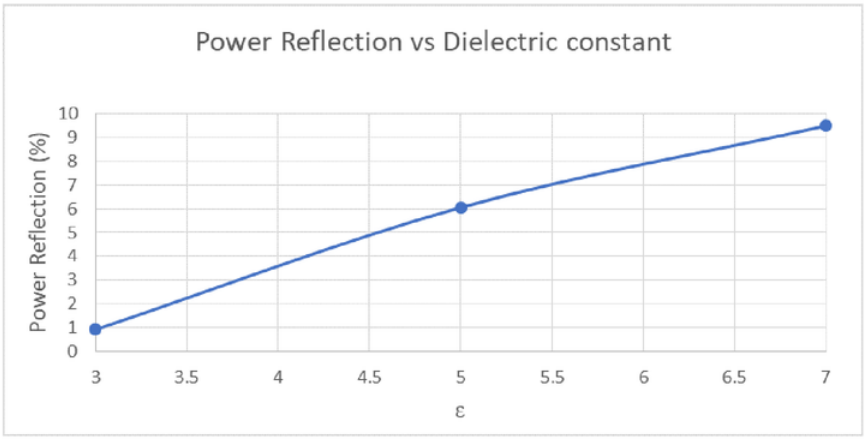

(b) Power Reflected by the test sample

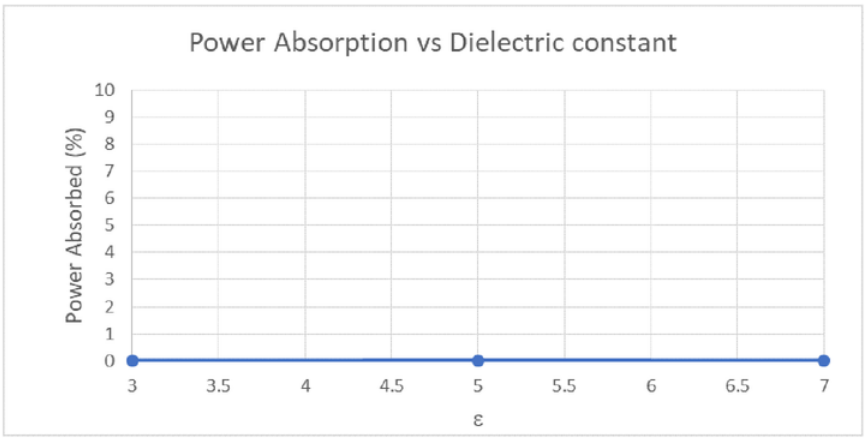

(c) Power Absorbed by the test sample

Figure 3.16: Power graphs of test sample with different dielectric constant

3.3.3 Test sample with different thickness

Thickness of the sample has a great impact on the amount of fields that can reflect and penetrate the sample. This section looks at test samples with different sample thickness

Test Sample specifications

- Dielectric constant (ϵ): 3
- Test Sample thickness: 50 nm, 1 μm, 1 mm
- Conductivity (σ): 1.6×10^{-3} $\frac{S}{m}$,

Power analysis

As the sample thickness is increased, there is more material for the fields to interact with (fields need to travel through more material to get to the other end of the open waveguide). These fields can either be absorbed or reflected by the charges within the sample. Figure 3.17 suggests that in this scenario, the reduction in output power in power transmission graph is due to these field being reflected back from the sample. Notice there is a no change in power absorption as the sample thickness is increased, however, as the sample thickness is increased drastically, there is high power reflection.

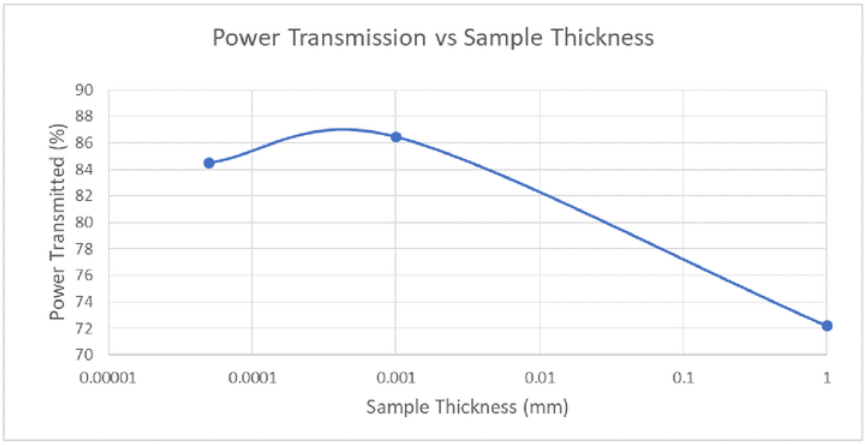

(a) Power Transmission in presence of test sample

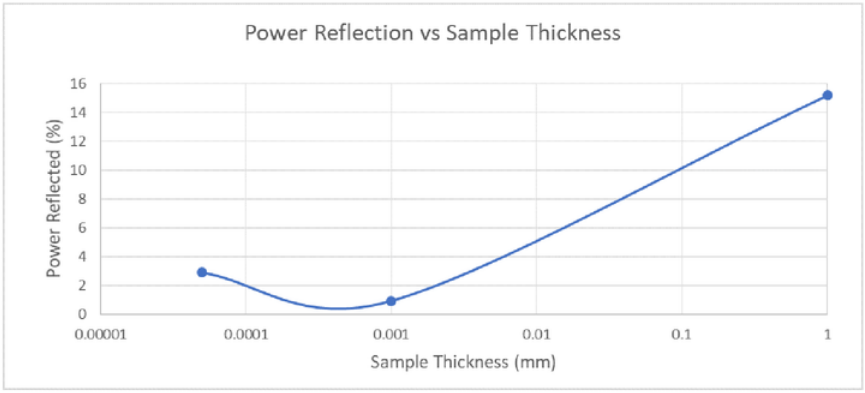

(b) Power Reflected by the test sample

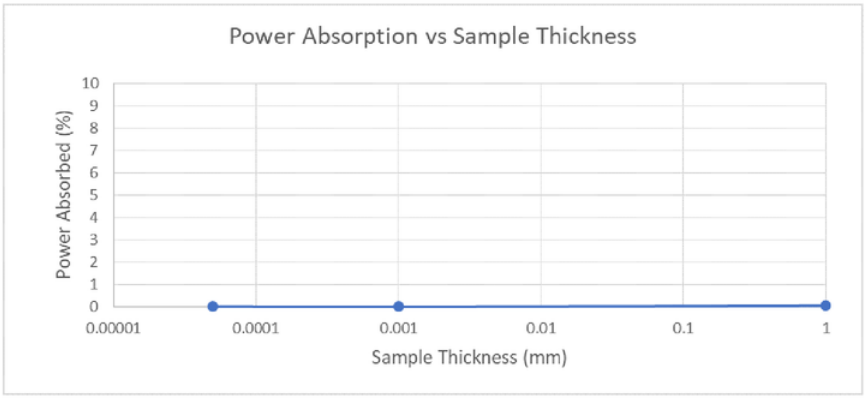

(c) Power Absorbed by the test sample

Figure 3.17: Power transmission, reflection and absorption by test sample with different thickness

Table 3.8: Test sample of different thickness in an open waveguide

Thickness (mm)	S11(dB)	S21(dB)	$P_{R(total)}$ (W)	$P_{T(total)}$ (W)	$P_{L(total)}$ (W)	$P_{R(sample)}$ (W)	$P_{A(sample)}$ (W)
0.00005	-8.2228	-0.7317	0.0752	0.4225	0.0022	0.0145	6.29E-5
0.001	-8.828	-0.6317	0.0654	0.4323	0.0022	0.0047	2.16E-5
1	-5.6332	-1.4159	0.1367	0.3609	0.0024	0.0758	0.0002

3.4 Conclusion

This chapter used WR90 open waveguide to simulate interaction between microwaves and sample material. Different configurations of waveguide was investigated to find the best suited waveguide configuration. After changing the waveguide material, length and wall thickness, it can be concluded that a brass waveguide of length 100mm and 0.5 wall thickness is appropriate for this thesis. Quartz and material with different conductivity, dielectric constant and thickness were simulated inside this waveguide to understand how each of these properties influence the power absorption, reflection and transmission of microwaves. As the conductivity of the material is increased, power absorbed by the material is gradually increased from 0% to 5%. Change in dielectric constant has very little impact on power absorption, but as the ϵ is increased, the material starts to reflect more power. This relationship is the same for sample with different thickness. At higher sample thickness, it reflects more power and the power absorption remains unchanged.

Chapter 4

Semiconductor materials in a Cavity

Previous chapter used rectangular waveguide to test semiconductors, the results obtained in this configuration can be considered as 'averaged' results because of the propagating waves, i.e. test samples were subjected to maximum, minimum and zero field. This chapter aims to use a configuration which can be used to obtain results when the sample is subjected to the maximum field. This can be achieved by using a cavity resonator, which can be constructed by closing the ports of the open waveguide. An ideal cavity is a closed box which stores electric and magnetic fields and has zero losses. The microwaves within the cavity bounce back and forth and at resonant frequency they form standing waves. [10]

4.1 Cavity Configurations

A rectangular cavity resonator is modelled using the previous WR90 waveguide configuration by closing one end of the waveguide such that the structure is left with just 1 port. This port acts as the input and output port. Iris is positioned inside the cavity such that only 1 wavelength is allowed inside. This condition is met for particular frequencies, known as resonant frequency. The resonant frequency for empty cavity is at 9 GHz. Two cavity models with different iris radius are investigated in this section and their model specifications are detailed below.

4.1.1 Cavity Model I

Cavity Model Specifications

- Inner Dimensions: a = 22.86 mm, b = 10.16 mm
- Length of the whole structure (z axis): 100 mm
- Number of ports: 1 (Note: Port 2 has been closed by using brass)
- Iris position along z axis: 48.2

- Iris thickness: 1 mm
- Iris radius: 5.08 mm
- Cavity wall thickness: 0.5 mm
- Material of the Cavity: Brass (91%)
- Material inside the cavity: Vacuum
- Iris material: Brass (91%) and Vacuum
- Input Power (P_I) = 0.5W

4.1.2 Cavity Model II

Cavity Model Specifications

- Inner Dimensions: a = 22.86 mm, b = 10.16 mm
- Length of the whole structure (z axis): 100 mm
- Number of ports: 1 (Note: Port 2 has been closed by using brass)
- Iris position along z axis: 48.2
- Iris thickness: 1 mm
- Iris radius: 4 mm
- Cavity wall thickness: 0.5 mm
- Material of the Cavity: Brass (91%)
- Material inside the cavity: Vacuum
- Iris material: Brass (91%) and Vacuum
- Input Power (P_I) = 0.5W

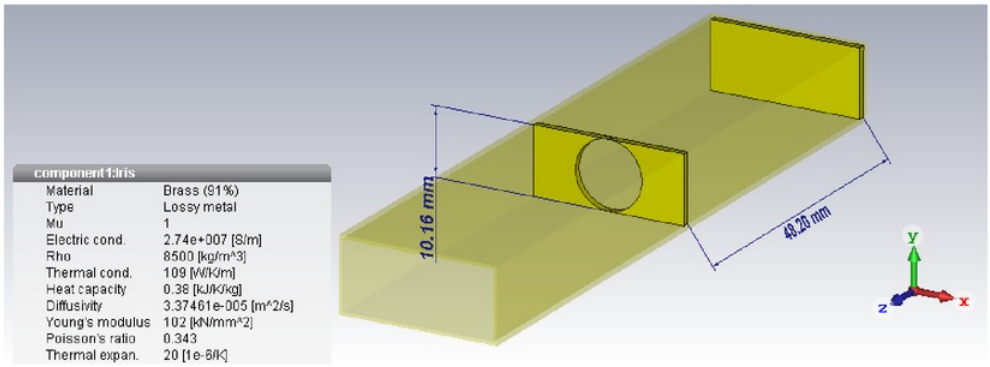

(a) Cavity Model I

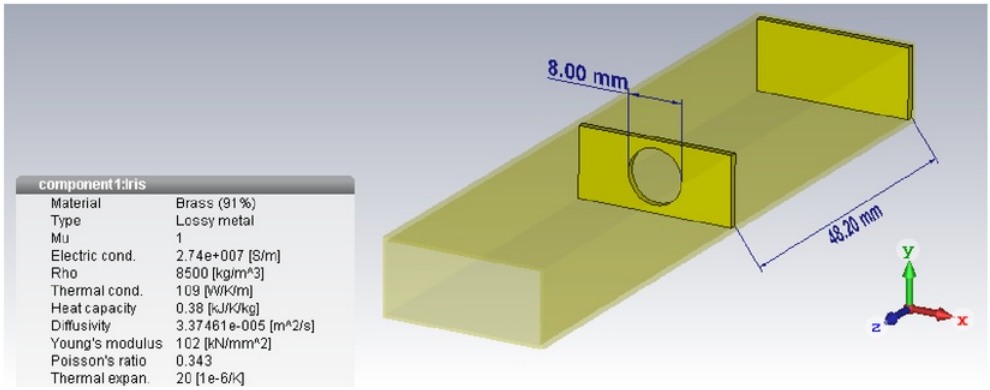

(b) Cavity Model II

Figure 4.1: Cavity Resonator model

4.1.3 Field Distributions

The E-field distribution in figure 4.2 are obtained from Cavity model I. The iris acts like a partially reflecting mirror that allows only certain frequency to enter the cavity and the rest are reflected back. This frequency is known as the resonant frequency and they can be varied by moving the iris placement. These field distributions clearly display the standing wave pattern (high concentration of E-fields) inside the cavity at frequency of 9 GHz. At 8.2 GHz, the fields are reflected back by the iris and hence the amplitude of the field are extremely low.

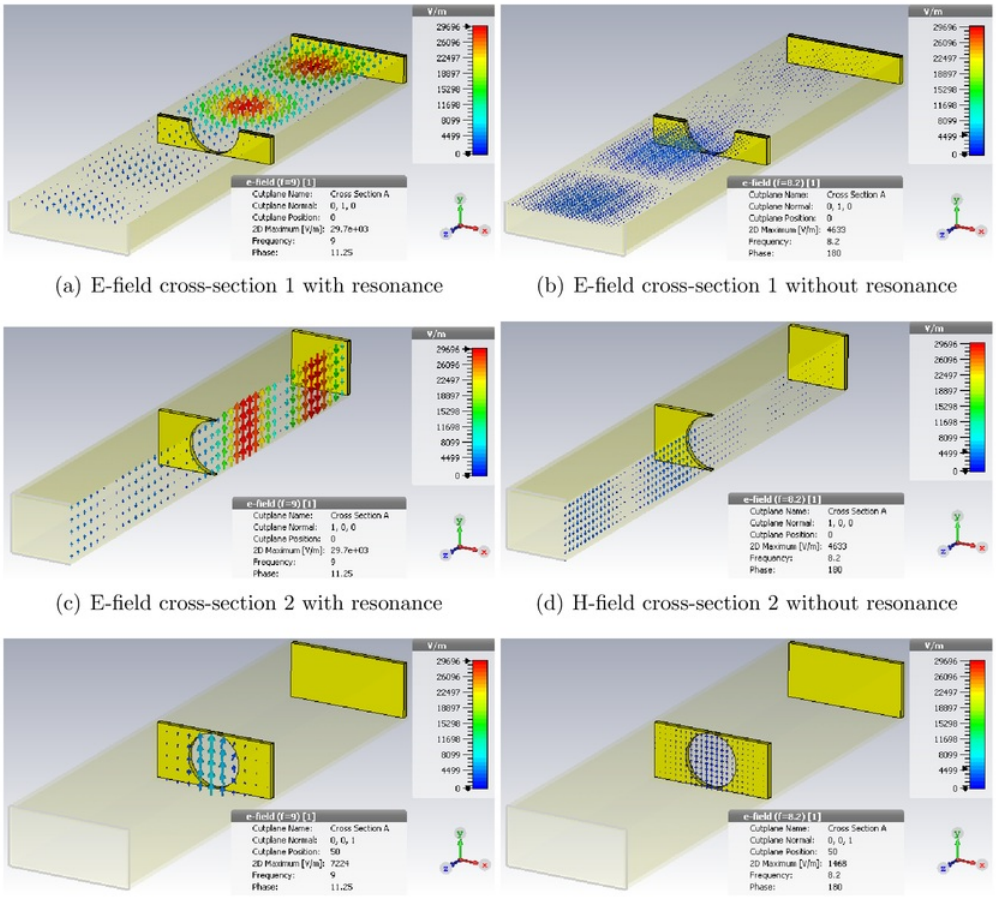

(a) E-field cross-section 1 with resonance

(b) E-field cross-section 1 without resonance

(c) E-field cross-section 2 with resonance

(d) H-field cross-section 2 without resonance

(e) E-field cross-section 3 with resonance

(f) H-field cross-section 3 without resonance

Figure 4.2: TE_{10} Field Distribution in Empty Cavity at different frequencies

4.2 Cavity with Quartz

Quartz specifications

- Inner Dimensions: a = 22.86 mm, b = 10.16 mm
- Quartz thickness: 1 mm
- Quartz placement (on z axis): 35 mm
- Material: Quartz (lossy)

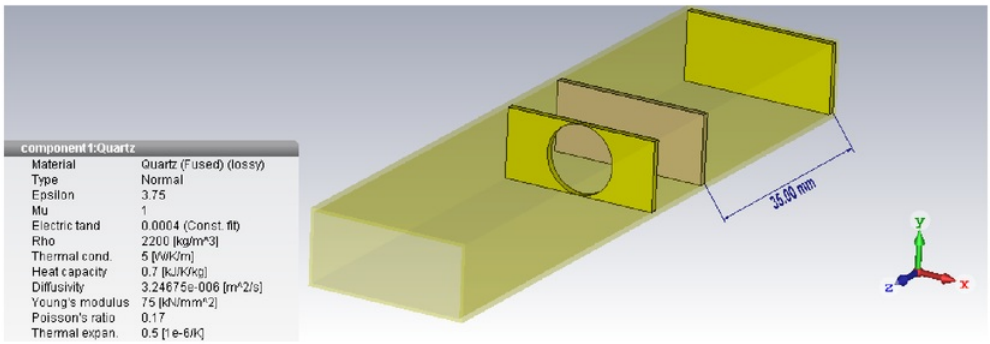

Figure 4.3: Cavity Model I with quartz placed at 35 mm on z axis

Field Distributions

Figure 4.4 shows the field distributions for cavity model I and II with quartz placed at the maximum field. Notice for Cavity model I, E-fields are more concentrated inside the cavity, but for cavity model II, most of the E-fields are reflected back even at resonance, due to small iris. The maximum e-field for cavity model I is 39.99e+03, such high field amplification can be achieved by superposition of two waves with same wavelength travelling in opposite direction. This forms a standing wave. Cavity model II has also formed standing wave but since most of the fields are reflected back due to small iris, the e-field maximum is much lower.

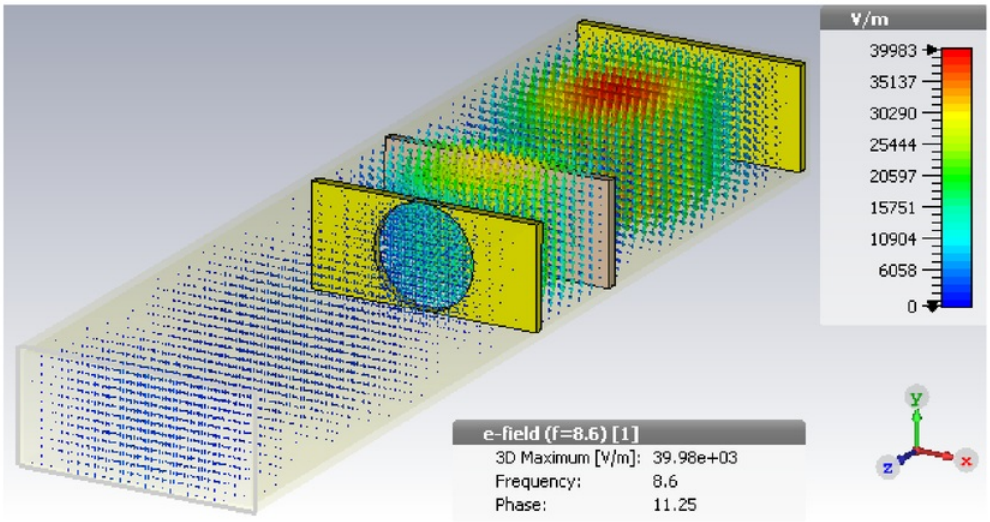

(a) Cavity Model I with quartz

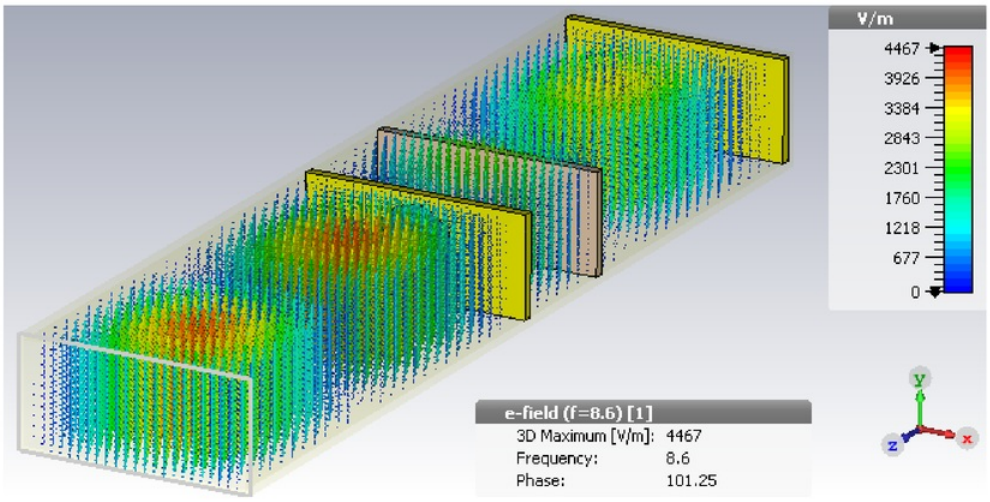

(b) Cavity Model II with quartz

Figure 4.4: E-Field distributions for cavity with quartz at their resonance

Power Analysis

The resonance curve of a microwave cavity is characterised by f_0, R_0 and ΔW. This curve has a depth of R_0, which is the minimum of the curve and occurs at resonant frequency (f_0). Full width at half maximum is represented by ΔW and the half-power frequencies occur at f_- and f_+. A visual illustration of this can be seen in figure 4.5. Cavity is characterised by the quality factor Q_L and response time τ_{RC}. Q_L represents the sharpness of the resonant curve, i.e. the higher Q_L, the sharper the resonance. [4]

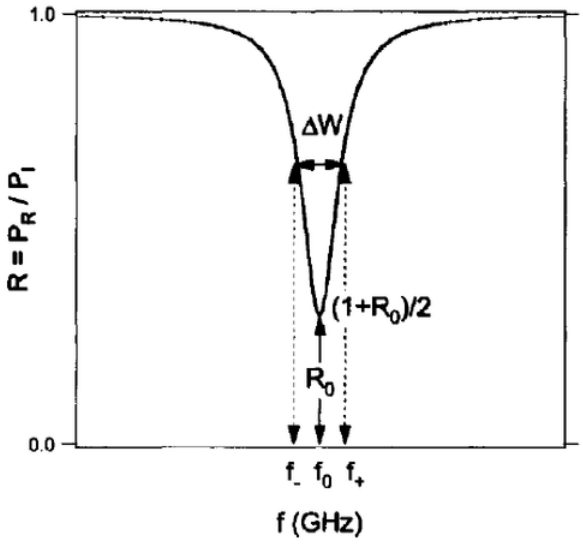

Figure 4.5: Resonance curve of a microwave cavity [4]

$$Q_L = \frac{f_0}{\Delta W} \tag{17}$$

$$\tau_{RC} = \frac{Q_L}{\pi f_0} \tag{18}$$

Two cavity models were investigated by varying the iris radius and to see its effect on the resonance curve. It is ideal to have cavity with small iris radius such that cavity will be of a higher quality (i.e. less power loss, and provides a better standing wave), however the input power to the cavity will also be low.

As it can be seen in Figure 4.6 and Table 4.1, iris radius of 4mm provides a high quality cavity and it would work very well for some samples but not all due to its extremely sharp resonance. Experimentally it would be really hard to tune to achieve right resonance. Very small changes can shift the resonance by a large factor which makes it hard to do

measurements, especially with such sharp resonances. Hence, following stages of this thesis will use cavity model I for testing. Notice, in cavity for frequencies other than the resonant frequency, the wavelength that not 'fit' inside the cavity. So, there iris reflects these fields of these frequencies back. At the resonant frequency, the field goes past the iris and are trapped inside the cavity forming standing waves. This introduces the loss and the curve shown in figure 4.6.

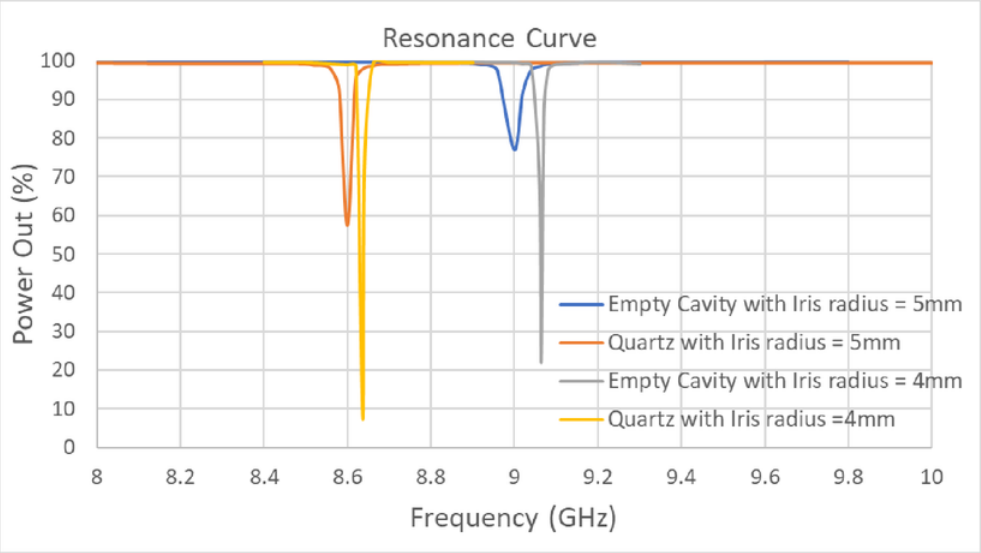

Figure 4.6: Resonance curves of cavity models with and without quartz

Table 4.1: Quantitative analysis of the resonance curves

Cavity type	Q_L	τ_{RC}
Empty Cavity (5mm iris radius)	225	7.9 ns
Empty Cavity (4mm iris radius)	1590	55 ns
Cavity with quartz (5mm iris radius)	330	12 ns
Cavity with quartz (4mm iris radius)	863.6	31 ns

4.3 Cavity with Test Sample

In this section, test samples with different electrical properties are deposited on top of quartz, inside the cavity and their P_{out} and P_A are analyzed. P_{out} is the total power reflected back to port 1 (input and output port). P_A is the power absorbed by the sample and is calculated in the way as shown in eq.15. However, since the loses in the cavity is

different to open waveguide, P_L (Quartz) inside the cavity is approximately 0.21 W which was found in previous section. All simulations performed in this section use cavity model I which was discussed in previous section.

4.3.1 Test samples with different conductivity

Test Sample specifications

- Test sample placement (along z axis): 36mm
- Dielectric constant (ϵ): 3
- Test Sample thickness: 1 μm
- Conductivity (σ): 1.6×10^{-6} $\frac{S}{m}$, 1.6×10^{-3} $\frac{S}{m}$, 1.6 $\frac{S}{m}$

Field Distribution

Figure 4.7 displays the E-field distributions inside the cavity model I with quartz and sample material placed at the maximum field. For sample with high conductivity, the cavity start losing its resonance.

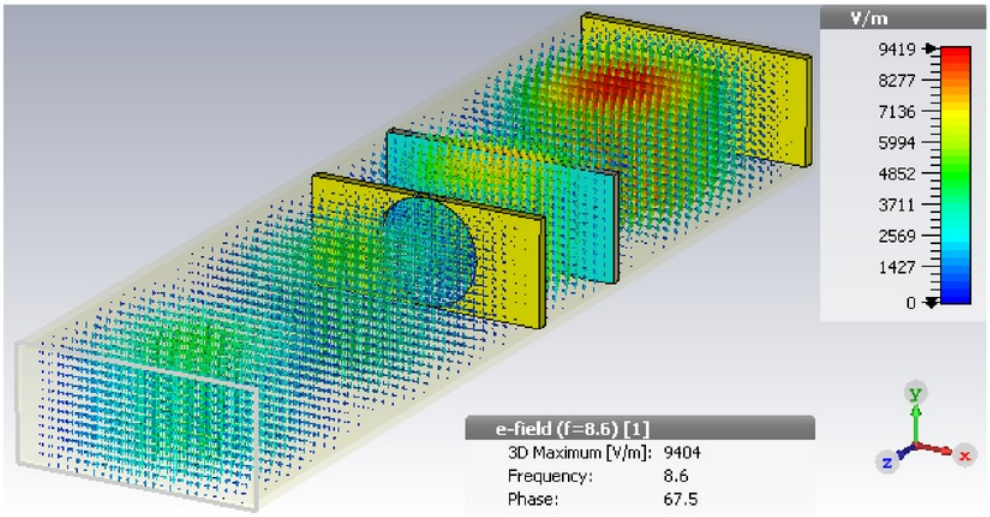

(a) Sample with Conductivity of 1.6×10^{-6} $\frac{S}{m}$

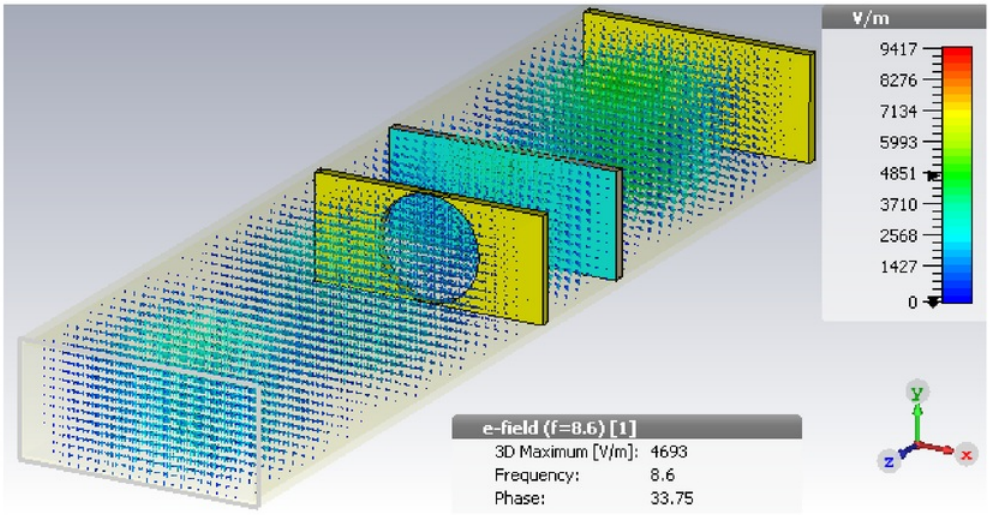

(b) Sample with Conductivity of 1.6 $\frac{S}{m}$

Figure 4.7: E-Field distribution for sample with different conductivity

Power Analysis

Increased conductivity implies high electron density, which gives a more imperfect cavity at conductivity of 1.6 S/m. This can be seen by the widening of the resonance curve in the figure 4.6. The resonance curve for 1.6×10^{-6} S/m and 1.6×10^{-3} S/m are overlapped. Their response can be clearly seen in figure 4.9, where the power absorption is increased with increasing conductivity. Using eq 17, Q_L for sample with conductivity of 1.6 S/m is 71.4 and Q_L for sample with conductivity of 1.6×10^{-6} S/m is 571.3. This suggests that for cavity with high conductivity sample has low quality. At conductivity of 1.6 S/m, output power is high which implies that power loss is low and this can be seen by the negative power absorption in figure 4.7, where the power loss with sample in the cavity is much lower than power loss with just quartz. However, technically it should be the other way around. Therefore, sample with highest conductivity (1.6 S/m) is behaving like a very thin metal which reflects most of the fields, this can be visually seen in figure 4.7 where the cavity has lost its resonance. Since the model loses its cavity at 1.6 S/m, the power absorption result obtained in figure 4.9 is negligible. This also indicates the limitation of this model where any conductivity equal to or higher than 1.6 S/m and with above sample configuration would not work in this model.

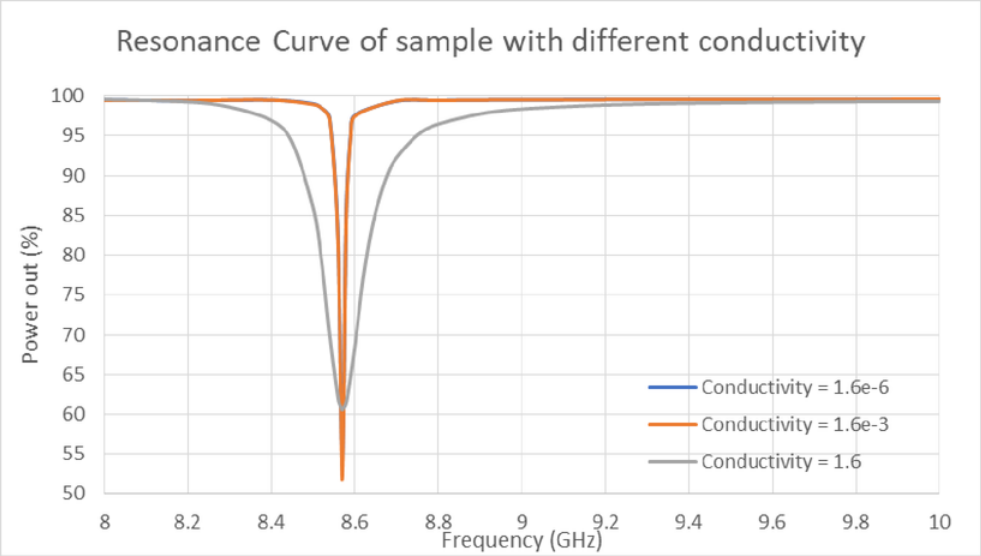

Figure 4.8: Resonance curves of test sample with different conductivity

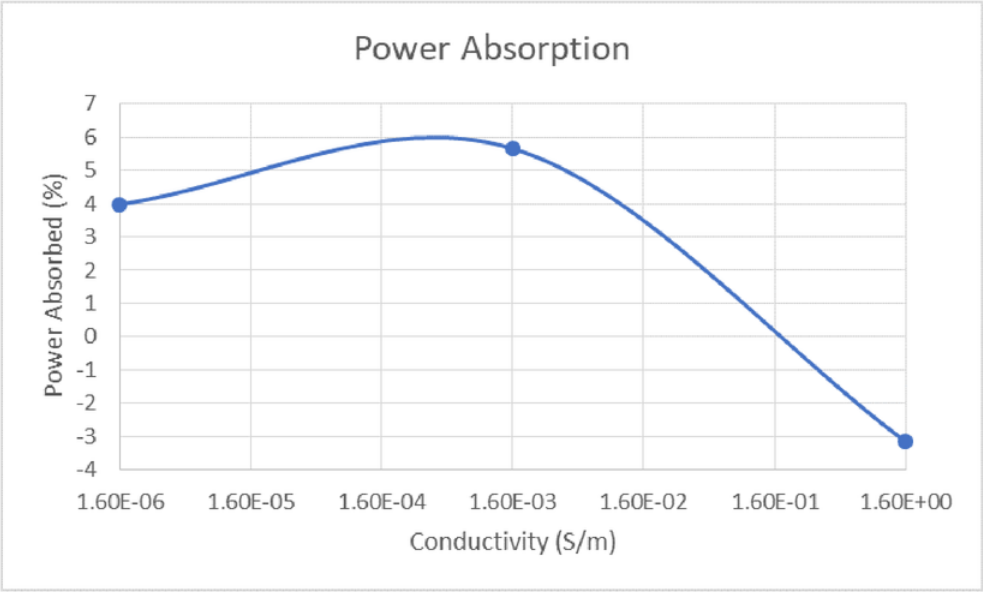

Figure 4.9: Power absorbed by the test sample with different conductivity

4.3.2 Test sample with different dielectric constant

Test Sample specifications

- Test Sample placement (along z axis): 36mm
- Dielectric constant (ϵ): 3, 5, 7
- Test Sample thickness: 1 μm
- Conductivity (σ): 1.6×10^{-3} $\frac{S}{m}$,

Power Analysis

Dielectric constant (ϵ) of the material effectively changes the path length in the cavity which increases the power loss in the cavity and hence increases the power absorption in the sample. This parameter varies the resonance of the cavity and this can be seen in figure 4.10, where the resonance is shifted as the ϵ is varied. Power absorption is increased with higher dielectric constant just as predicted because, higher dielectric constant indicates that the charges can easily be pulled apart and this relationship can be seen in figure 4.11.

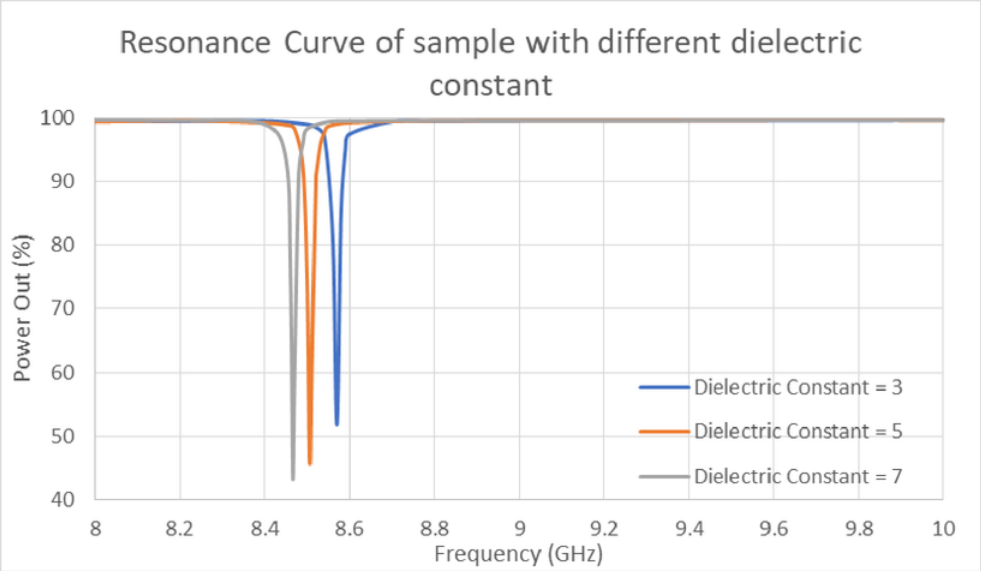

Figure 4.10: Resonance curves of test sample with different dielectric constant

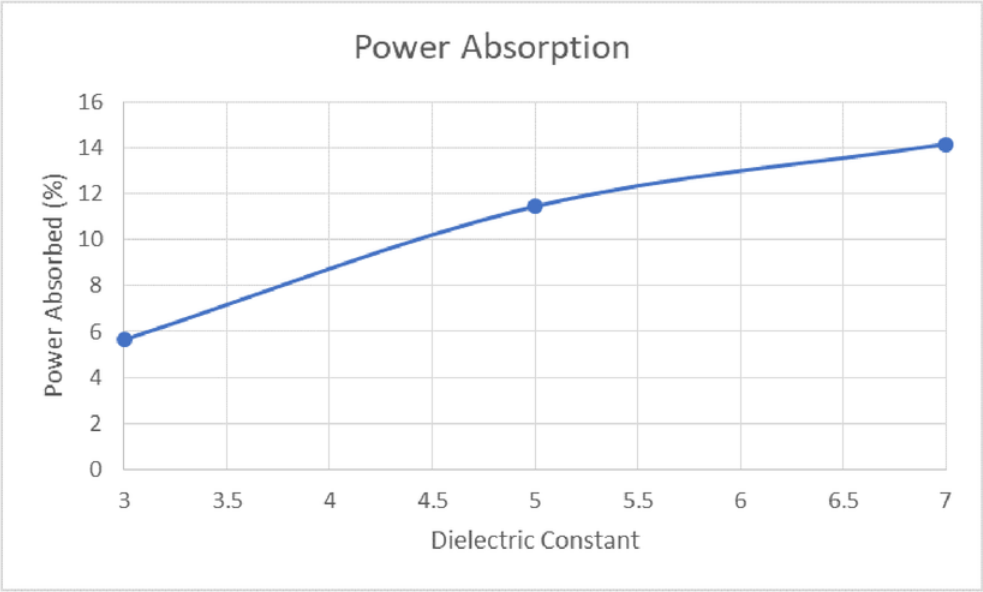

Figure 4.11: Power absorbed by the test sample with different dielectric constant

4.3.3 Test sample with different thickness

Test Sample specifications

- Test Sample placement (along z axis): 36mm
- Dielectric constant (ϵ): 3
- Test Sample thickness: 200 nm, 500 nm, 1 μm, 2 μm
- Conductivity (σ): 1.6×10^{-3} $\frac{S}{m}$,

Power Analysis

Figure 4.12 illustrates the resonance curves for test samples of various thickness. The resonance curves for samples thickness 200nm to 1 μm is the same however for 2μm the output power is increased. Thin samples allow the microwaves to easily travel through the material, however samples with larger thickness like 2 μm, make it hard for the microwave fields to travel through the sample, this obstruction causes higher reflection.

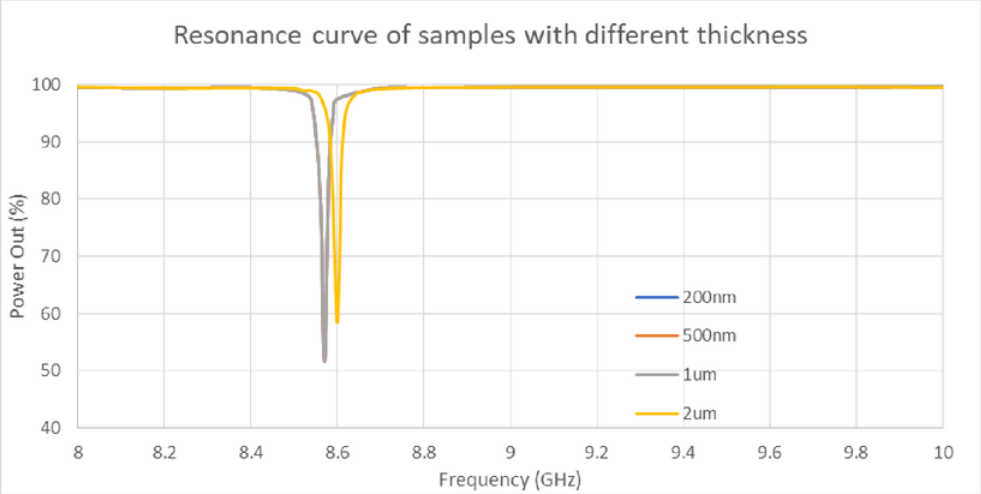

Figure 4.12: Resonance curves of test sample with different thickness

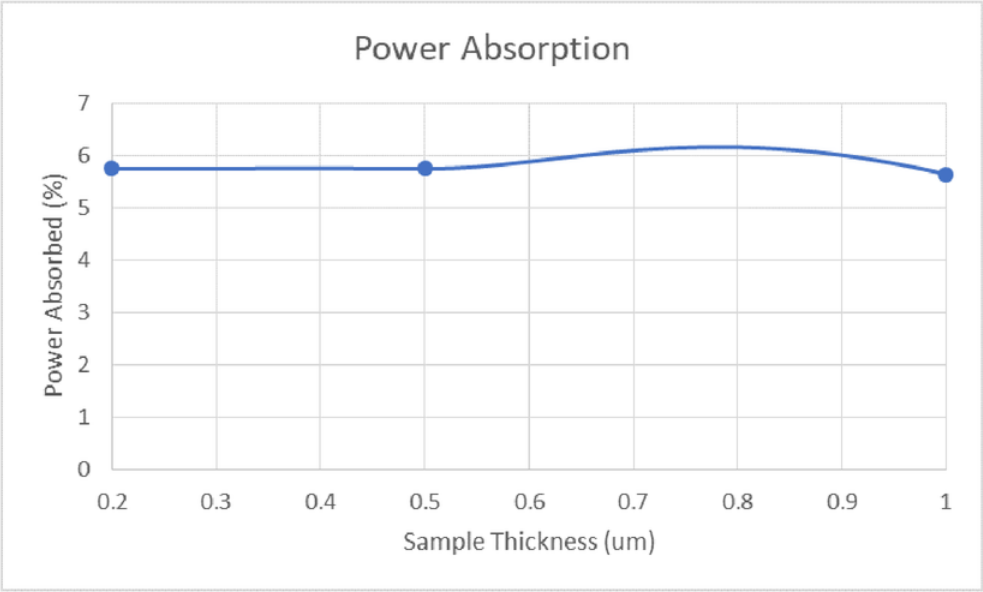

Figure 4.13: Power absorbed by the test sample with different thickness

4.4 Cavity with Real Photovoltaic Samples

This section investigates the interaction between microwaves and real photovoltaic materials when they are deposited on top of quartz in cavity model I. The real PV materials investigated in this section are OPV, Silicon, Cadmium Telluride and Gallium Arsenide. The conductivity of these materials are varied by changing the doping of the material. Up until now, all the models used T solver to simulate the models. Since the complexity of the model has increased, all the models from this section onwards, will use frequency domain solver with tetrahedral mesh type.

4.4.1 OPV

Material Specification

- Test sample placement (along z axis): 36mm
- Dielectric constant ($\frac{\epsilon_s}{\epsilon_0}$): 3.5
- Test Sample thickness: 1 μm
- Mobility: $\mu_n = 1 \times 10^{-7} m^2/Vs$ and $\mu_p = 1 \times 10^{-8} m^2/Vs$
- Conductivity (σ): Refer to Table 4.2

Table 4.2: Material conductivity of OPV with respect to n-p doping

Doping (n-p) (m^{-3})	Conductivity ($\frac{S}{m}$)
1×10^{19}	1.76×10^{-7}
1×10^{20}	1.76×10^{-6}
1×10^{21}	1.76×10^{-5}
1×10^{22}	1.76×10^{-4}

Field Distribution

Figure 4.14 displays the E-field distributions inside the cavity model I with quartz and OPV material placed at the maximum field. E-field does not change as the conductivity of the OPV is varied. This supports the power graphs shown figure 4.15 and 4.16.

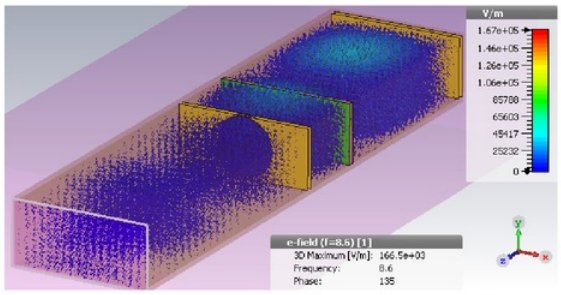

(a) OPV with Conductivity of 1.76×10^{-7} $\frac{S}{m}$

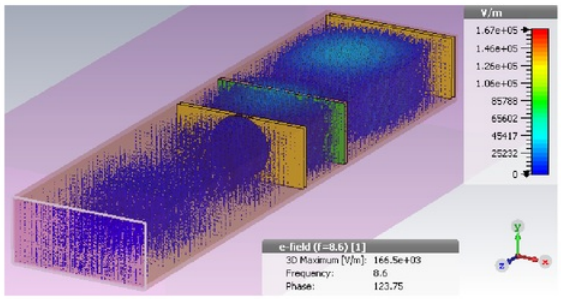

(b) OPV Conductivity 1.76×10^{-6} $\frac{S}{m}$

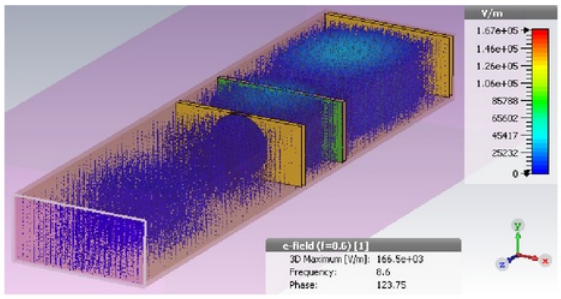

(c) OPV Conductivity 1.76×10^{-5} $\frac{S}{m}$

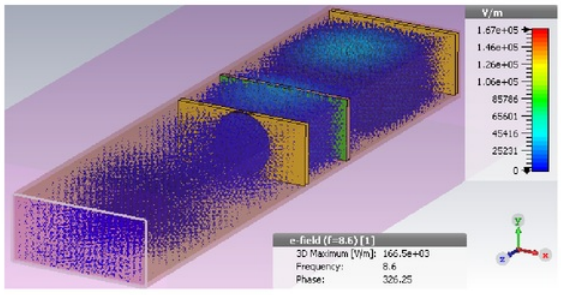

(d) OPV Conductivity 1.76×10^{-4} $\frac{S}{m}$

Figure 4.14: E-Field distribution for OPV with different conductivity

Power Analysis

Figure 4.15 shows the resonance curves for OPV with different conductivities and these curves are overlapped suggesting that these materials have the same response. This is more clearly shown in figure 4.16 where the power absorption is the same for all conductivities. They have the same response because the conductivity of the materials being simulated here are extremely low. Real difference in their response can be seen in the next chapter where the conductivity of OPV is higher due to photoconductivity elements. The resonance curves of OPV with low conductivity has Q_L of about 330.

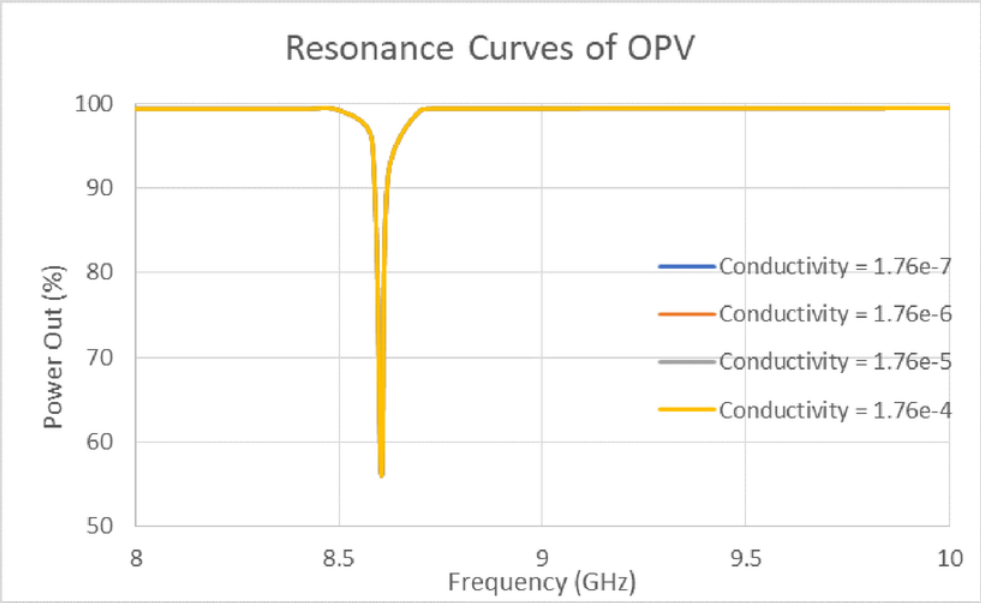

Figure 4.15: Resonance curves of OPV with different conductivity

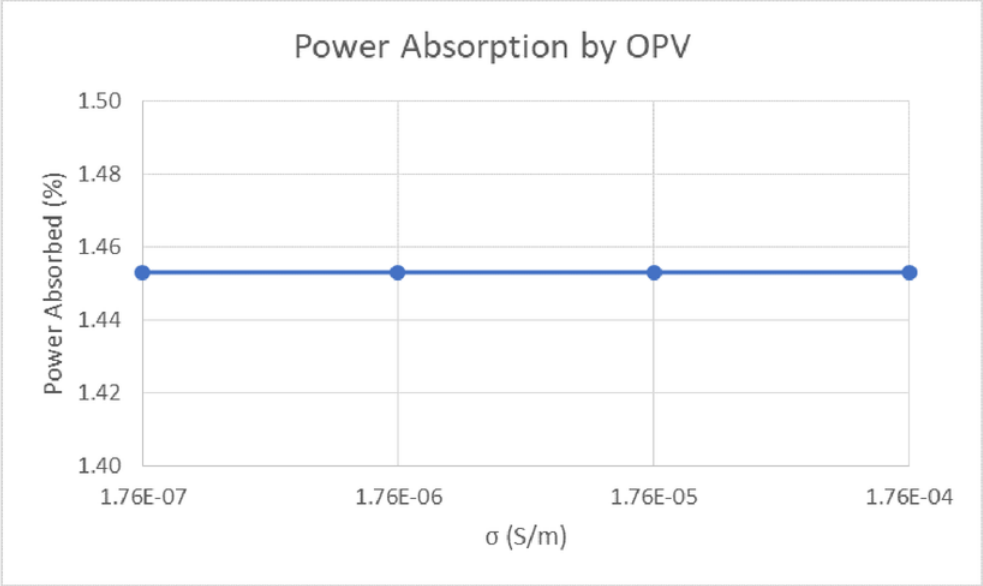

Figure 4.16: Power absorbed by OPV with different conductivity

4.4.2 Silicon

Material Specification

- Test sample placement (along z axis): 36mm
- Dielectric constant ($\frac{\epsilon_s}{\epsilon_0}$): 11.9
- Test Sample thickness: 1 μm
- Mobility: $\mu_n = 0.145\ m^2/Vs$ and $\mu_p = 0.05\ m^2/Vs$
- Conductivity (σ): Refer to Table 4.3

Table 4.3: Material conductivity of Silicon with respect to n-p doping

Doping (n-p) (m^{-3})	Conductivity ($\frac{S}{m}$)
1×10^{19}	0.312
1×10^{20}	3.12
1×10^{21}	13.2
1×10^{22}	132

Field Distribution

Figure 4.17 displays the E-field distribution for the cavity model with silicon materials of different conductivities. As the conductivity is increased (due to high doping), more e-fields can be seen on the outside of the cavity. At high conductivity, silicon reflects some of the e-fields which in turn increases the field density outside the cavity and decreases the amplitude of the resulting field inside the cavity. This can be seen in figure 4.17 (a), e-field maximum is 75.29e+03 V/m for conductivity of 0.312 S/m and in figure 4.17 (d), e-field maximum is 5597 V/m for conductivity of 312 S/m. Even though the input power for all these models are the same, the reflected fields is out of phase with the input fields, which cancels out or reduces the resulting amplitude of e-field as shown in figure 4.17 (d).

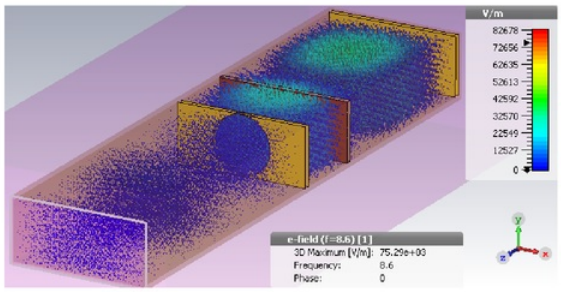

(a) Silicon with Conductivity of 0.312 $\frac{S}{m}$

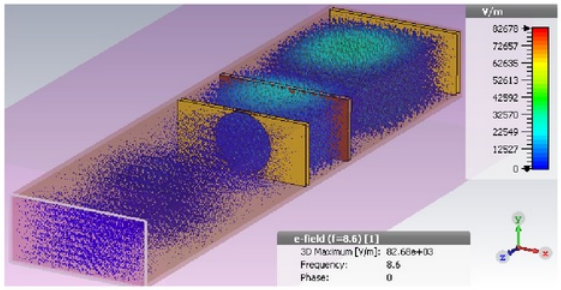

(b) Silicon Conductivity 3.12 $\frac{S}{m}$

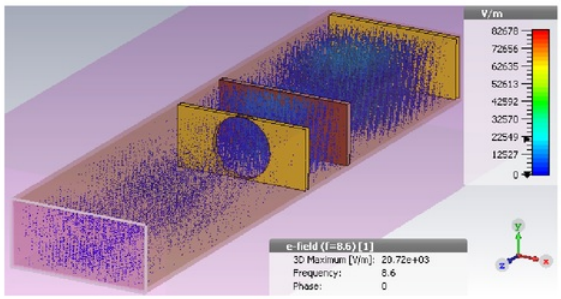

(c) Silicon Conductivity 31.2 $\frac{S}{m}$

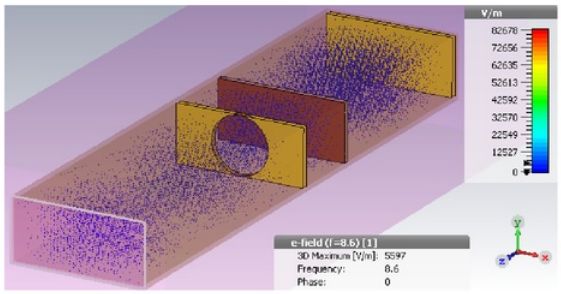

(d) Silicon Conductivity 312 $\frac{S}{m}$

Figure 4.17: E-Field distribution for Silicon with different conductivity

Power Analysis

Resonance curves of silicon with different conductivity can be seen in figure 4.18. As the conductivity is increased, the resonance curve starts widening. Widening of resonance curve relates the quality of the cavity. Sharp resonance indicates that the cavity is of high quality and its near perfect. At conductivity of 0.312, cavity has Q_L of 330 and at conductivity of 31.2 the quality of the cavity drops to 40. So, at higher conductivity, cavity is more imperfect. Figure 4.19 indicates that power absorbed by the silicon is increased as the conductivity is increased. At extremely high conductivity (312 S/m), the sample shorts the cavity by reflecting most of the power. Hence, the power absorption is not calculated for this scenario.

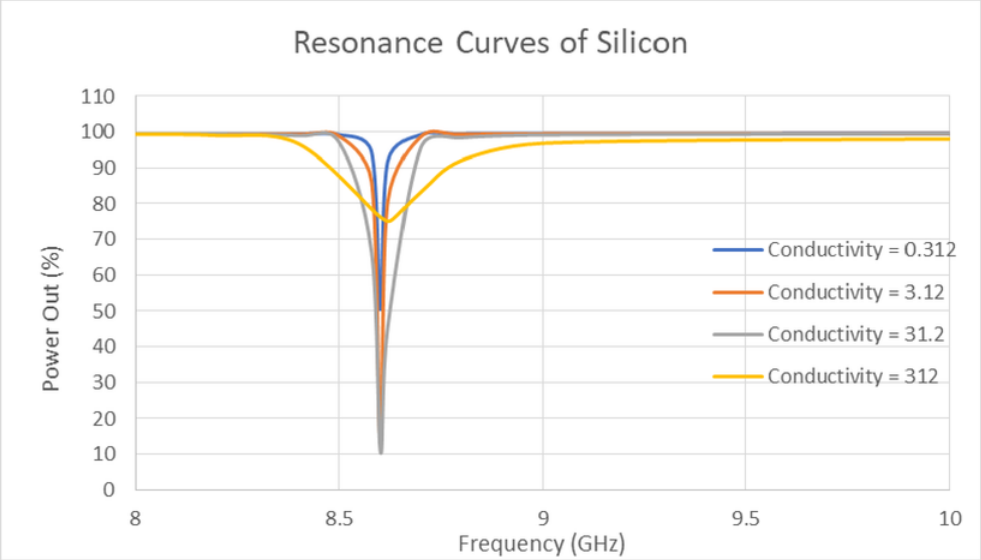

Figure 4.18: Resonance curves of Silicon with different conductivity

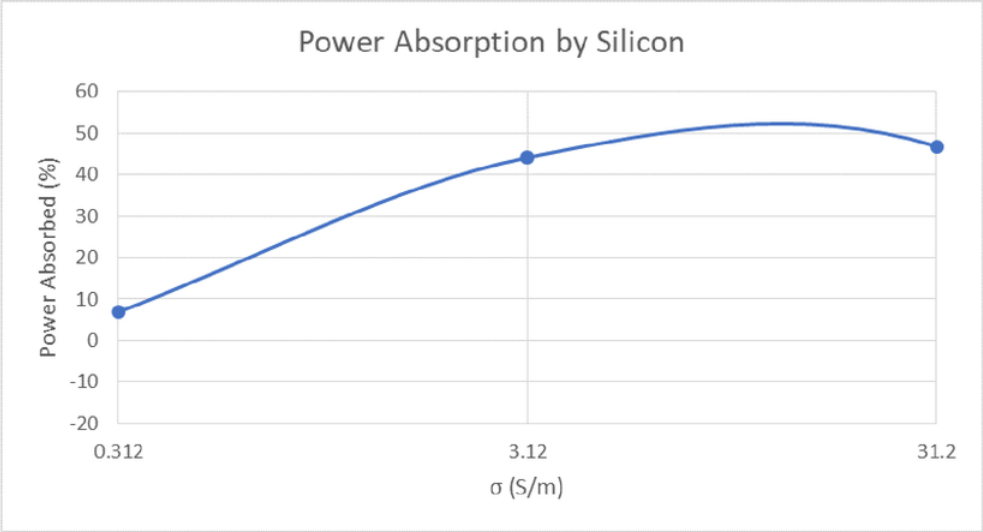

Figure 4.19: Power absorbed by Silicon with different conductivity

4.4.3 Cadmium Telluride

Material Specification

- Test sample placement (along z axis): 36mm
- Dielectric constant ($\frac{\epsilon_s}{\epsilon_0}$): 10.2
- Test Sample thickness: 1 μm
- Mobility: $\mu_n = 0.105\ m^2/Vs$ and $\mu_p = 0.01\ m^2/Vs$
- Conductivity (σ): Refer to Table 4.4

Table 4.4: Material conductivity of CdTe with respect to n-p doping

Doping (n-p) (m^{-3})	Conductivity ($\frac{S}{m}$)
1×10^{19}	0.184
1×10^{20}	1.84
1×10^{21}	18.4
1×10^{22}	184

Field Distribution

Figure 4.20 displays the E-field distribution for the cavity model with CdTe materials of different conductivities. As the conductivity is increased, more e-fields can be seen on the outside of the cavity. At high conductivity CdTe reflects some of the e-fields which in turn increases the field density outside the cavity and decreases the amplitude of the resulting field inside the cavity. This can be seen in figure 4.20 (a), e-field maximum is 85.26e+03 V/m for conductivity of 0.184 S/m and in figure 4.20 (d), e-field maximum is 5584 V/m for conductivity of 184 S/m.

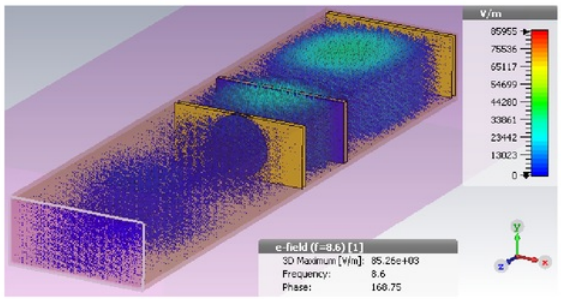

(a) CdTe with Conductivity of 0.184 $\frac{S}{m}$

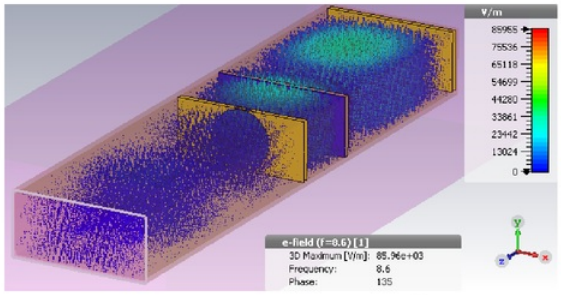

(b) CdTe Conductivity 1.84 $\frac{S}{m}$

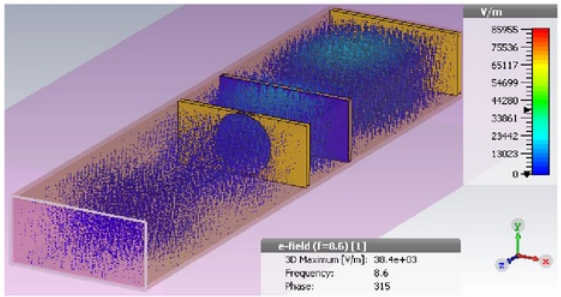

(c) CdTe Conductivity 18.4 $\frac{S}{m}$

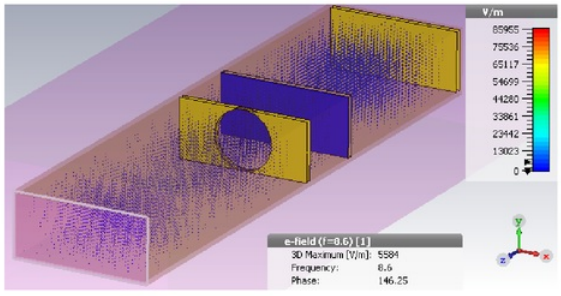

(d) CdTe Conductivity 184 $\frac{S}{m}$

Figure 4.20: E-Field distribution for CdTe with different conductivity

Power Analysis

Resonance curves of CdTe with different conductivity can be seen in figure 4.21. As the conductivity is increased, the resonance curve starts widening. Widening of resonance curve indicates the quality of the cavity. Sharp resonance indicates that the cavity is of high quality and its near perfect. So, at higher conductivity, cavity is more imperfect. Figure 4.22 indicates that power absorbed by the CdTe is increased as the conductivity is increased. At extremely high conductivity (184 S/m), the sample shorts the cavity by reflecting most of the power. Hence, the power absorption is not calculated for this scenario.

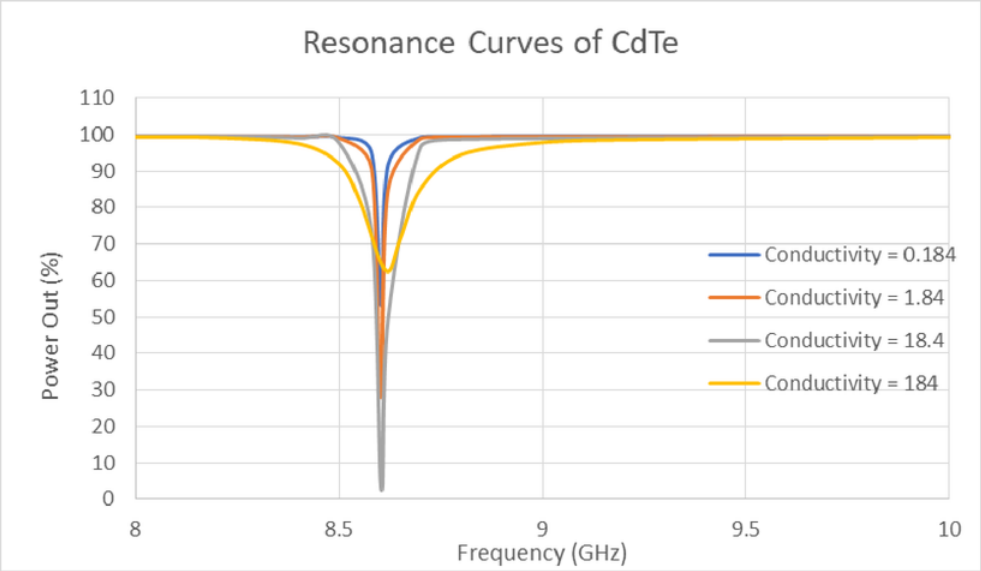

Figure 4.21: Resonance curves of CdTe with different conductivity

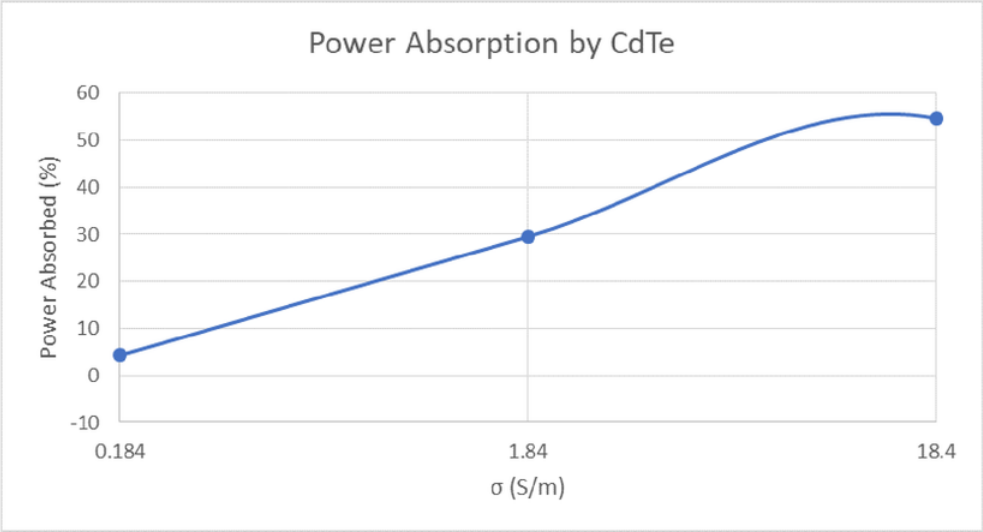

Figure 4.22: Power absorbed by CdTe with different conductivity

4.4.4 Gallium Arsenide

Material Specification

- Test sample placement (along z axis): 36mm
- Dielectric constant ($\frac{\epsilon_s}{\epsilon_0}$): 12.9
- Test Sample thickness: 1 μm
- Mobility: $\mu_n = 0.8\ m^2/Vs$ and $\mu_p = 0.04\ m^2/Vs$
- Conductivity (σ): Refer to Table 4.5

Table 4.5: Material conductivity of GaAs with respect to n-p doping

Doping (n-p) (m^{-3})	Conductivity ($\frac{S}{m}$)
1×10^{19}	1.344
1×10^{20}	13.44
1×10^{21}	134.4
1×10^{22}	1344

Field Distribution

Figure 4.23 illustrates the e-field distributions of GaAs with different conductivities. GaAs behaves very similar to silicon and CdTe, where the e-fields are reflected back as the material conductivity is increased. However, GaAs for highest doping (1×10^{22}) has extremely high conductivity when compared to OPV, silicon and CdTe. Due to this high conductivity, extremely small fraction of e-field enter the cavity and the rest are reflected back. This can be seen in figure 4.23 (d) and the highest amplitude for this model is 4485 V/m which is much lower than any other materials discussed previously.

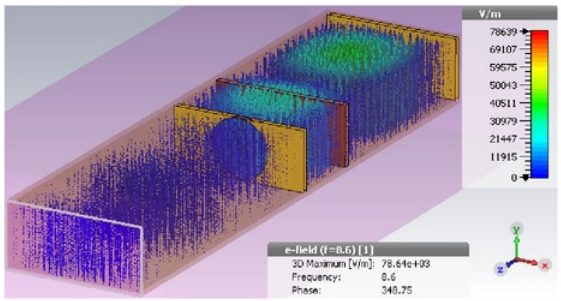

(a) GaAs with Conductivity of 1.344 $\frac{S}{m}$

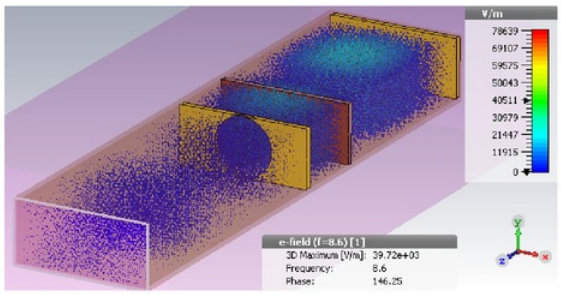

(b) GaAs Conductivity 13.44 $\frac{S}{m}$

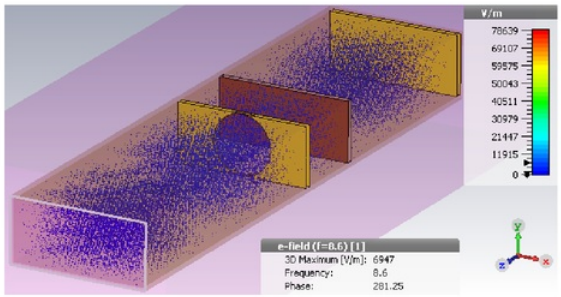

(c) GaAs Conductivity 134.4 $\frac{S}{m}$

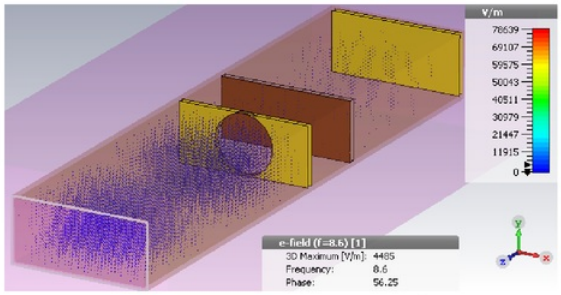

(d) GaAs Conductivity 1344 $\frac{S}{m}$

Figure 4.23: E-Field distribution for GaAs with different conductivity

Power Analysis

Figure 4.24 has the resonance curves of GaAs with different conductivities. At highest conductivity, the model has almost lost its resonance due to high reflection. Due to this fact, power absorption has not been plotted for this conductivity in figure 4.25. At low conductivity, the material has minimal power absorption, at medium conductivity (13.44 S/m), the material reaches its highest power absorption. Power absorption drops close to zero for conductivity of 134 S/m.

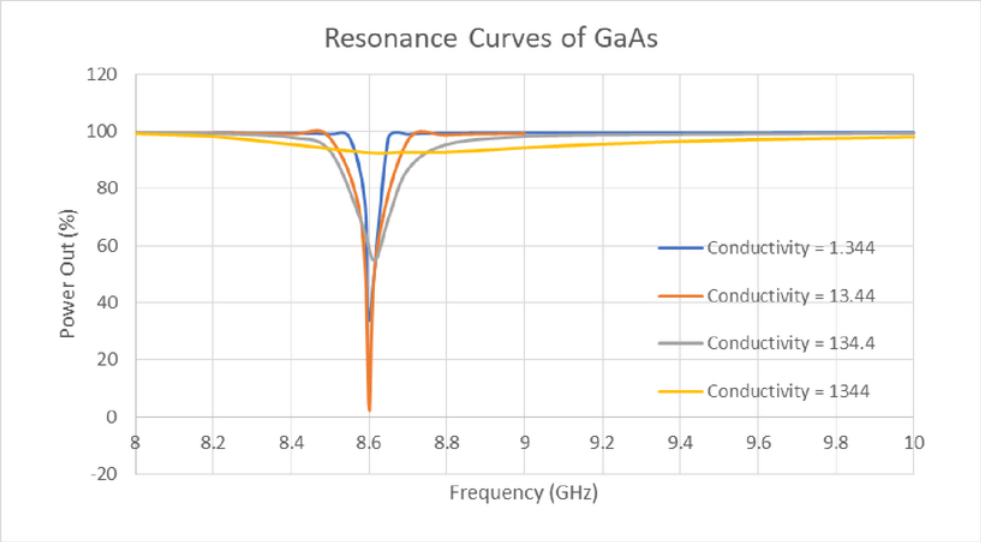

Figure 4.24: Resonance curves of GaAs with different conductivity

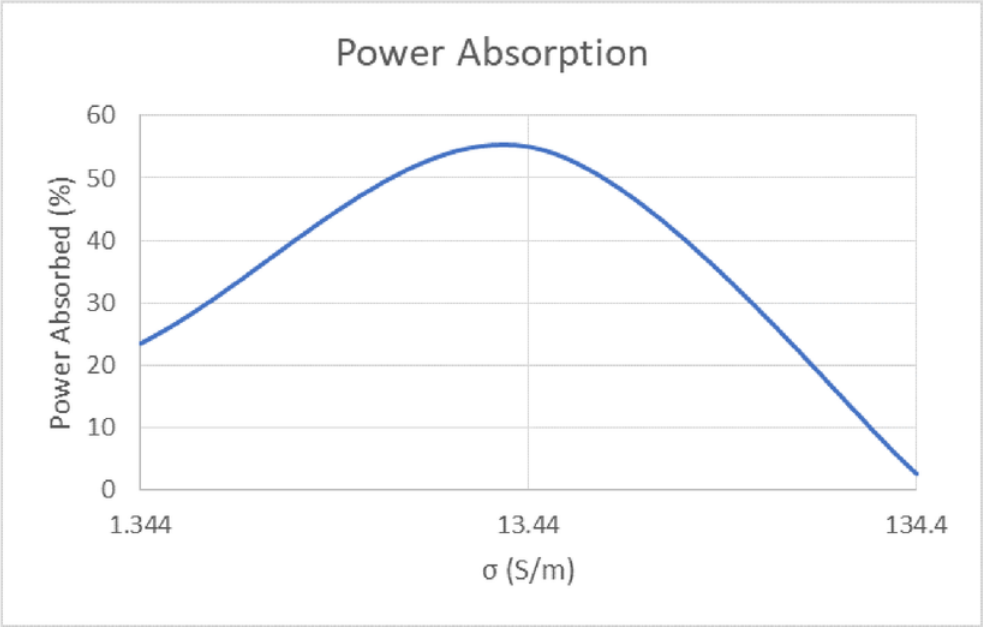

Figure 4.25: Power absorbed by GaAs with different conductivity

4.5 Conclusion

Two different cavity models were investigated and after analysing the functionality and suitability, Cavity model I was better suited. All the simulation carried out in this chapter uses cavity model I. In a vacuum filled cavity, when the iris is placed at 48.2 mm along z axis, it has resonance frequency at 9 GHz. Placing quartz and sample materials inside the cavity shifts this resonance depending on the dielectric constant. Different sample materials with varying conductivity, dielectric constant and thickness was placed inside the cavity to see the effect it can have on the resonance curve. Material with different conductivities widens or narrows the resonance curve, material with different dielectric constant shifts the resonance frequency. Conductivity, dielectric constant and the material thickness affects the power absorption of the material. Real photovoltaic samples were placed in the cavity to see their interaction with microwaves when there is no light flash. Conductivities of OPV, Silicon, CdTe and GaAs were varied by changing the doping of the material. For low doping, GaAs has the highest conductivity and OPV has the lowest. Change in material doping has very little to no impact on power absorption by the OPV. At highest doping (i.e. highest conductivity), Silicon, CdTe and GaAs start to lose their resonance in their cavity as they behave like mirror reflecting most of the microwaves. Therefore, samples with high dark conductivity and in particular, Silicon, CdTe and GaAs with 10^{22} m^{-3} doping and higher cannot be used for this model.

Chapter 5

Photoconductivity

In chapters 3 and 4, all the simulations were performed in dark (i.e. simulation model setup had no light flashing element to it, just material on its own, in the cavity or waveguide). This chapter investigates photoconductivity of the sample by flashing light onto its surface. Since this is a simulation model, for simplicity and to reduce the complexity of the model setup, light flashing is achieved by increasing the conductivity of the sample. Flashing light on to photovoltaic material is essentially giving the material extra energy which excites the charges within.

Note:

- σ_{dark}: conductivity of the material when there is no light
- σ_{light}: conductivity of the material when there is light
- $\delta\sigma$: photoconductivity (light flash)

$$\sigma_{light} = \sigma_{dark} + \delta\sigma \tag{19}$$

$$P_{light} = P_{dark} + \delta P \tag{20}$$

The photoconductivity of the samples are plotted in terms of normalised power level ($\delta P/P$) vs photoconductivity ($\delta\sigma$). These parameters are related by the expression shown in eq. 21, where K is the sensitivity or calibration factor.

$$\delta P/P = -K\delta\sigma \tag{21}$$

5.1 Test Samples

5.1.1 Material 1

Material with σ_{dark} of 1.6×10^{-3} $\frac{S}{m}$ (without light) is simulated to find resonance frequency, which is at 8.57 GHz. This frequency is fixed and rest of the simulation is carried by

changing the conductivity of the material according to σ_{light} values as shown in table 5.1 and the power readings are obtained at this frequency. This material is simulated using cavity model I which was discussed in chapter 4.

Material Specifications

- Test Sample placement (along z axis): 36mm
- Dielectric constant (ϵ): 3
- Test Sample thickness: 1 μm
- Conductivity (σ_{light}): Refer to Table 5.1

Table 5.1: Conductivity of the material 1 when the light is flashed onto it

σ_{dark}	$\delta\sigma$	σ_{light}
1.6×10^{-3}	0	1.6×10^{-3}
1.6×10^{-3}	1.6×10^{-3}	3.2×10^{-3}
1.6×10^{-3}	1.6×10^{-2}	0.0176
1.6×10^{-3}	1.6×10^{-1}	0.1616
1.6×10^{-3}	1.6	1.6

Field Distribution

Figure 5.1 illustrates the e-field distributions of material with different conductivities. At σ_{light} of 3.2×10^{-3} $\frac{S}{m}$, the cavity has a good resonance where the amplitude of e-field is about 9410 V/m and very small factor of e-fields are lost or reflected back. At σ_{light} of 1.6 $\frac{S}{m}$, the cavity is starting to lose its resonance and this can be seen by the reduction in amplitude to 4690 V/m and a lot more e-fields are reflected back.

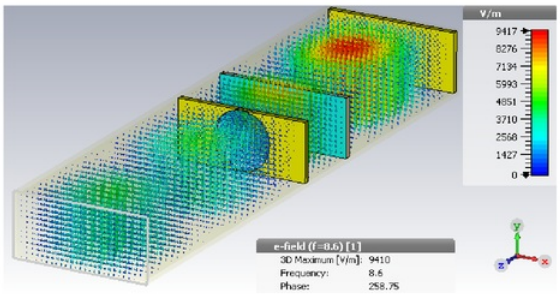

(a) Sample with Conductivity of 3.2×10^{-3} $\frac{S}{m}$

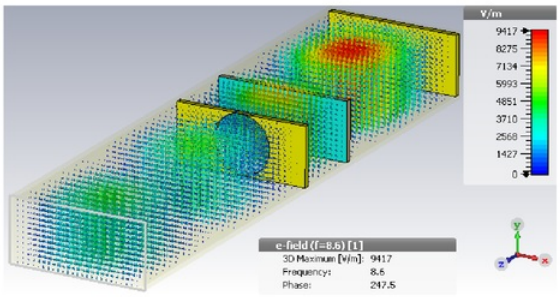

(b) Sample with Conductivity of 1.6×10^{-2} $\frac{S}{m}$

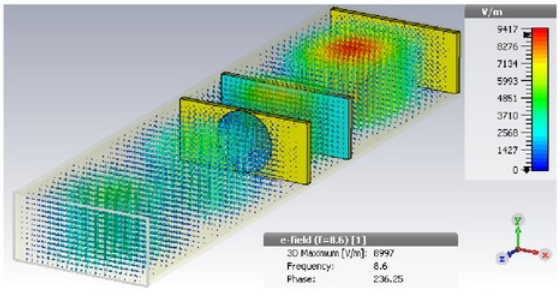

(c) Sample with Conductivity of 1.6×10^{-1} $\frac{S}{m}$

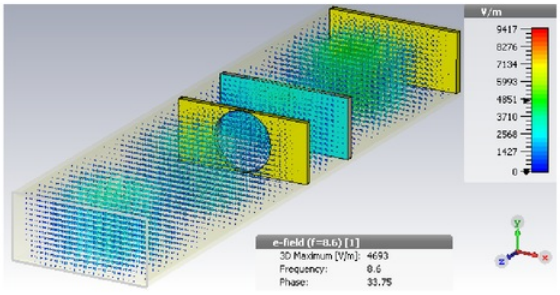

(d) Sample with Conductivity of 1.6 $\frac{S}{m}$

Figure 5.1: E-Field distribution for material 1 with different photoconductivity

Power Analysis

Figure 5.2 shows photoconductivity of material 1, where δP/P is the normalized power level. As the intensity of the light ($\delta\sigma$) being flashed on to the material is increased, the normalised power reaches 1. Once the light intensity becomes too high, the material starts to reflect more power, which reduces the normalized power. Figure 5.2 shows the power absorption by the material as the $\delta\sigma$ is increased. The material absorbs 58% of the power when the $\delta\sigma$ is 100 times greater than its σ_{dark}. For any higher intensity, the charges in the material has already reached its maximum excitation and it starts to reflect power rather than absorb which can be seen by the field distribution in figure 5.1. The sensitivity factor, K, is approximately 17.36 and its calculated from eq. 21.

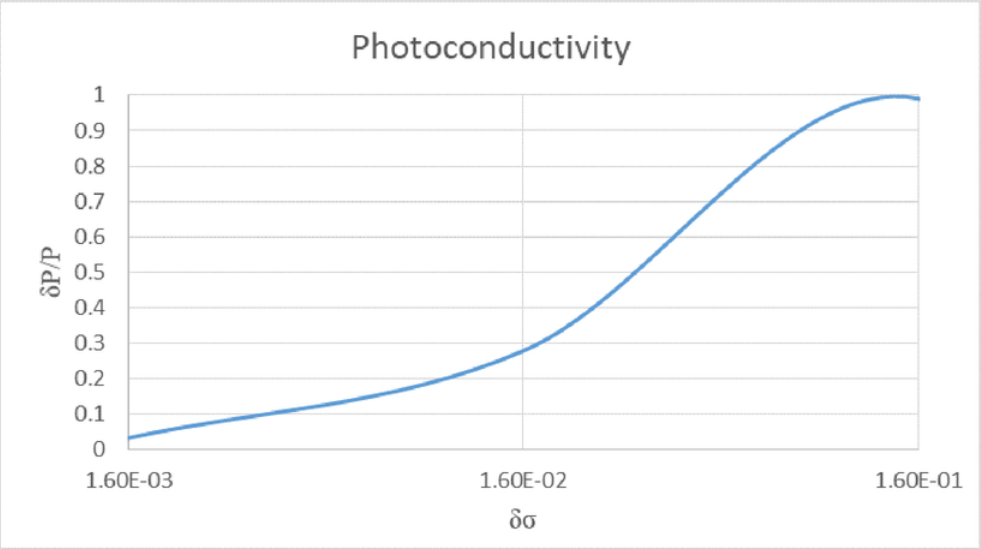

Figure 5.2: Photoconductivity of material 1

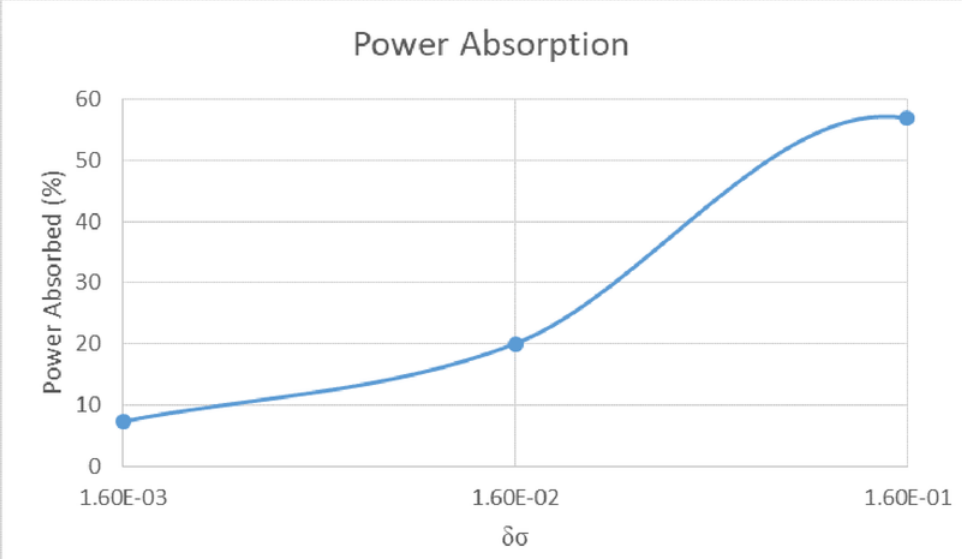

Figure 5.3: Power absorbed by material 1

5.1.2 Material 2

Material with σ_{dark} of 1.6×10^{-6} $\frac{S}{m}$ (without light) is simulated to find resonance frequency, which is at 8.57 GHz. This frequency is fixed and rest of the simulation is carried by changing the conductivity of the material according to σ_{light} values as shown in table 5.2 and the power readings are obtained at this frequency. This material is simulated using cavity model I which was discussed in chapter 4.

Material Specifications

- Test Sample placement (along z axis): 36mm
- Dielectric constant (ϵ): 3
- Test Sample thickness: 1 μm
- Conductivity (σ_{light}): Refer to Table 5.2

Table 5.2: Conductivity of the material 2 when the light is flashed onto it

σ_{dark}	$\delta\sigma$	σ_{light}
1.6×10^{-6}	0	1.6×10^{-6}
1.6×10^{-6}	1.6×10^{-6}	3.2×10^{-6}
1.6×10^{-6}	1.6×10^{-5}	1.76×10^{-5}
1.6×10^{-6}	1.6×10^{-4}	1.6×10^{-4}
1.6×10^{-6}	1.6×10^{-3}	1.6×10^{-3}
1.6×10^{-6}	1.6×10^{-2}	1.6×10^{-2}
1.6×10^{-6}	1.6×10^{-1}	1.6×10^{-1}
1.6×10^{-6}	1.6	1.6

Field Distribution

Figure 5.4 illustrates the e-field distributions of material 2 with different conductivities. At σ_{light} of 3.2×10^{-6} $\frac{S}{m}$, the cavity has a good resonance where the amplitude of e-field is about 9404 V/m and very small factor of e-fields are lost or reflected back. At σ_{light} of 1.6 $\frac{S}{m}$, the cavity is starting to lose its resonance and this can be seen by the reduction in amplitude to 4693 V/m and a lot more e-fields are reflected back.

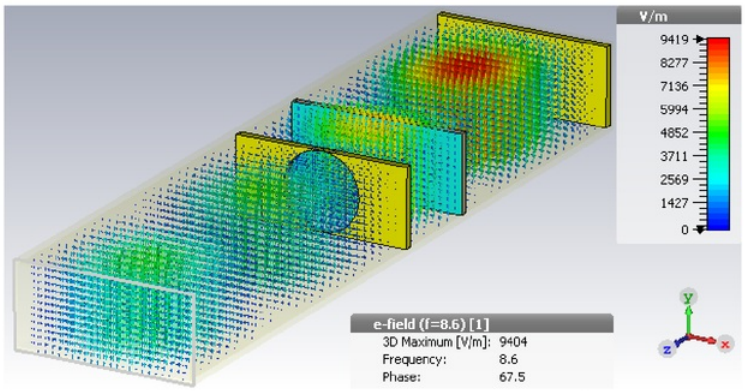

(a) Sample with Conductivity of 3.2×10^{-6} $\frac{S}{m}$

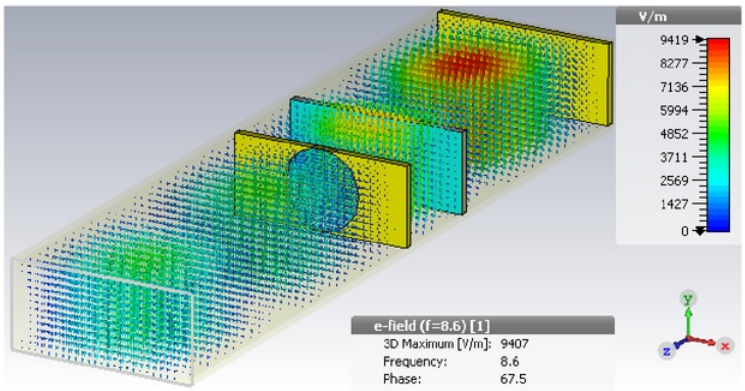

(b) Sample with Conductivity of 1.6×10^{-3} $\frac{S}{m}$

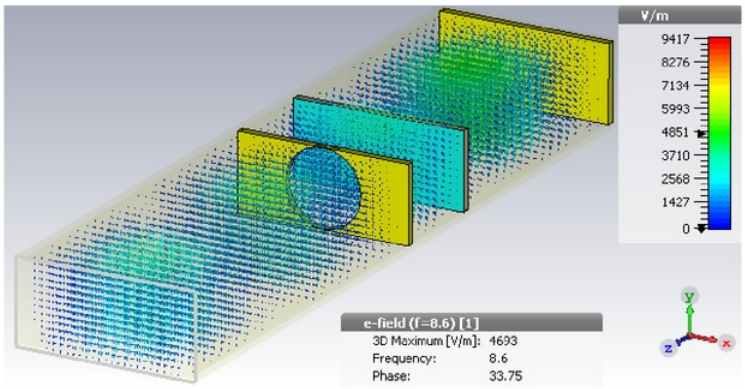

(c) Sample with Conductivity of 1.6 $\frac{S}{m}$

Figure 5.4: E-Field distribution for material 2 with different photoconductivity

Power Analysis

Figure 5.5 shows the photoconductivity of material 2. When $\delta\sigma$ is similar to σ_{dark}, the normalized power remains extremely low. δP is the change in output power with and without light. So, when the $\delta\sigma$ is low, output power with light is close to the output power when there is no light. Real difference can be seen when $\delta\sigma$ is 1000 times greater than σ_{dark}. Highest power absorption for this material occurs when $\delta\sigma$ is 10^5 times greater than the material conductivity. This can be seen in figure 5.7. The sensitivity factor, K, is approximately 20.83.

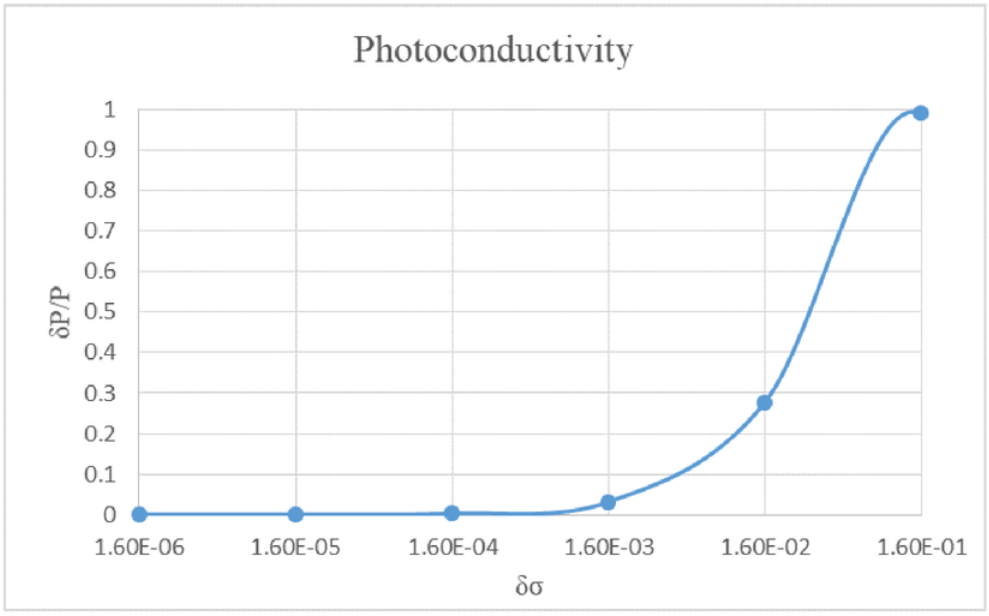

Figure 5.5: Photoconductivity of material 2

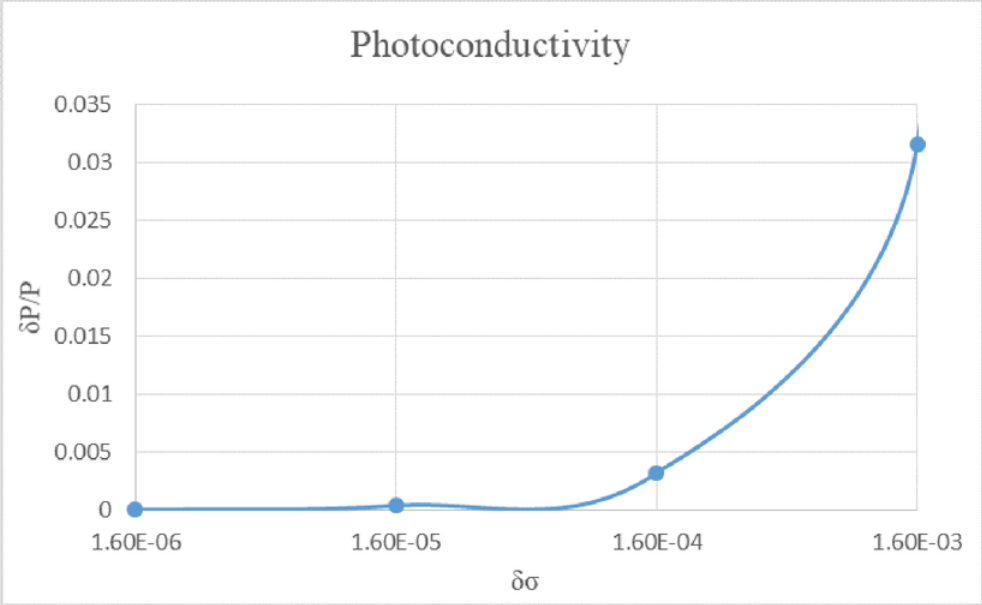

Figure 5.6: Photoconductivity of material 2 zoomed in to see the flat region from Figure 5.5

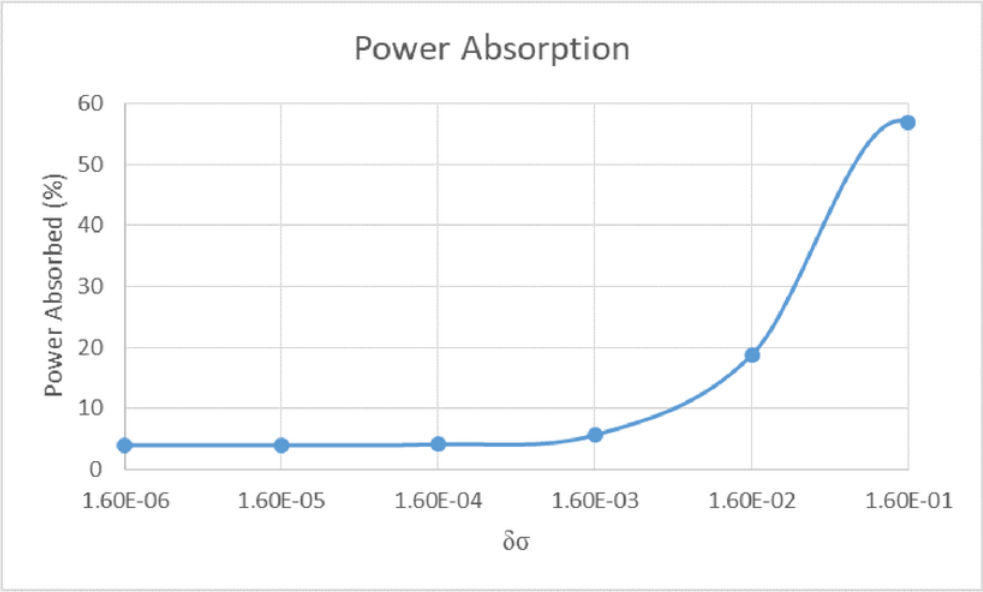

Figure 5.7: Power absorbed by material 2

5.2 Real Photovoltaic Samples

5.2.1 OPV

OPV material simulated in this section has σ_{dark} of 1.76×10^{-7} $\frac{S}{m}$. This is the lowest conductivity OPV material simulated in Chapter 4 and it has resonance frequency at 8.604 GHz. This frequency is fixed and the rest of the simulation is carried out by changing the conductivity of the material according to σ_{light} values as shown in table 5.3 and the power readings are obtained at this frequency. This material is simulated using cavity model I which was discussed in chapter 4.

Material Specification

- Test sample placement (along z axis): 36mm
- Dielectric constant ($\frac{\epsilon_s}{\epsilon_0}$): 3.5
- Test Sample thickness: 1 μm
- Mobility: $\mu_n = 1 \times 10^{-7} m^2/Vs$ and $\mu_p = 1 \times 10^{-8} m^2/Vs$
- Conductivity (σ_{light}): Refer to Table 5.3

Table 5.3: Material conductivity of OPV when light is flashed onto it

Doping (δn and δp) (m^{-3})	σ_{light} ($\frac{S}{m}$)
1×10^{22}	1.76×10^{-4}
1×10^{25}	1.76×10^{-1}
1×10^{28}	176

Field Distribution

Figure 5.8 illustrates the e-field distributions of OPV with different conductivities. Previously in section 4.4.1, the field distributions for this sample remained the same irrespective of the change in their conductivity. Now, the total conductivity of the material is much higher than the one discussed in chapter 4 due to light being flashed onto the material. This has increased the total conductivity of the OPV and hence, there is a slight variation in the e-fields. At σ_{light} of 1.76×10^{-4} $\frac{S}{m}$, the cavity has a good resonance where the amplitude of e-field is about 166.5×10^3 V/m and very small factor of e-fields are lost or reflected back. At σ_{light} of 177 $\frac{S}{m}$, the cavity still has a good resonance but the amplitude of e-field is reduced to 11.2×10^3 V/m and a lot more e-fields are reflected back and they can be seen outside the cavity on the other side of the iris.

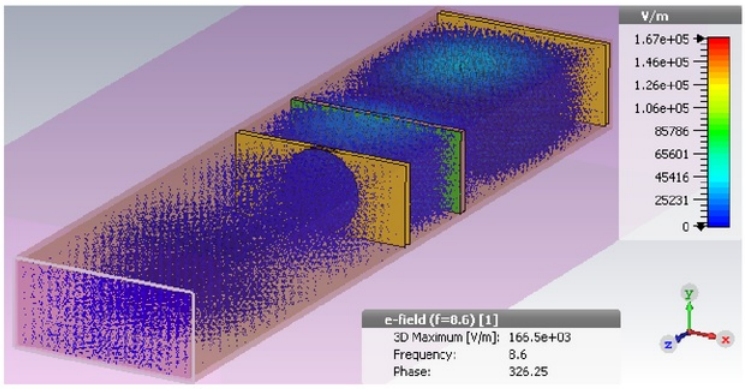

(a) OPV with Conductivity of 1.76×10^{-4} $\frac{S}{m}$

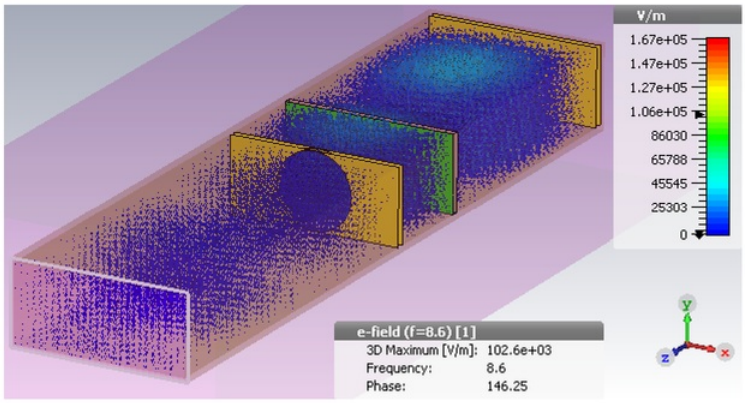

(b) OPV Conductivity 1.76×10^{-1} $\frac{S}{m}$

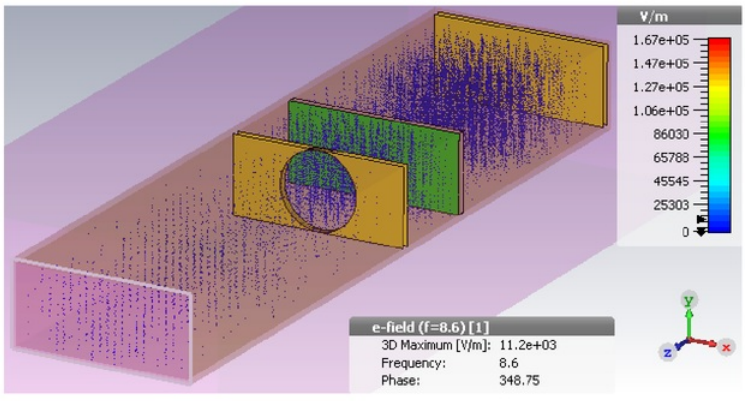

(c) OPV Conductivity 176 $\frac{S}{m}$

Figure 5.8: E-Field distribution for OPV with different photoconductivity

Power Analysis

Figure 5.9 shows the photoconductivity of OPV and figure 5.10 shows the power absorption. As the $\delta\sigma$ reaches higher than 0.176, OPV starts to reflect most of its power. OPV absorbs 6% of power when $\delta\sigma$ is 0.176. The sensitivity factor, K, is approximately 0.45.

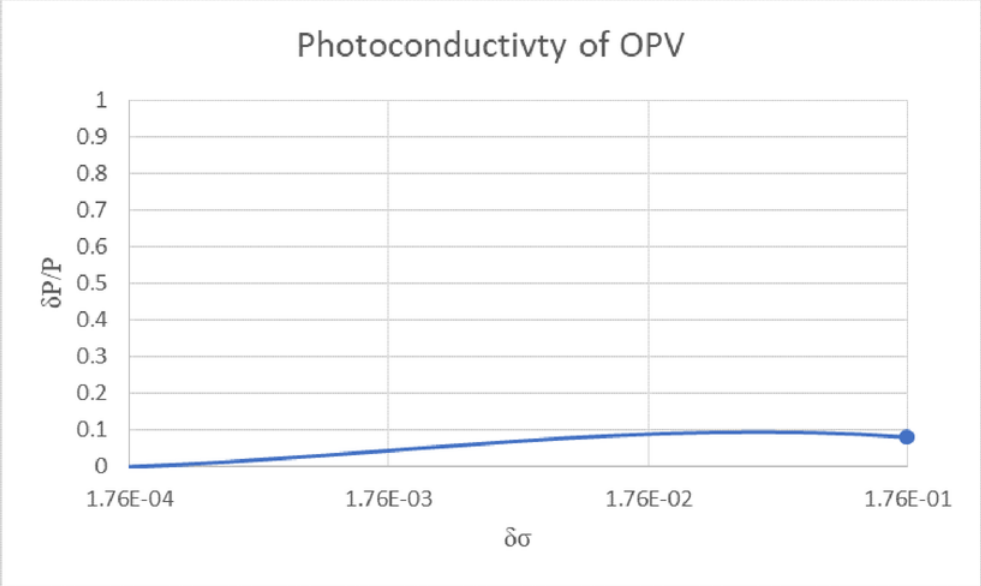

Figure 5.9: Photoconductivity of OPV

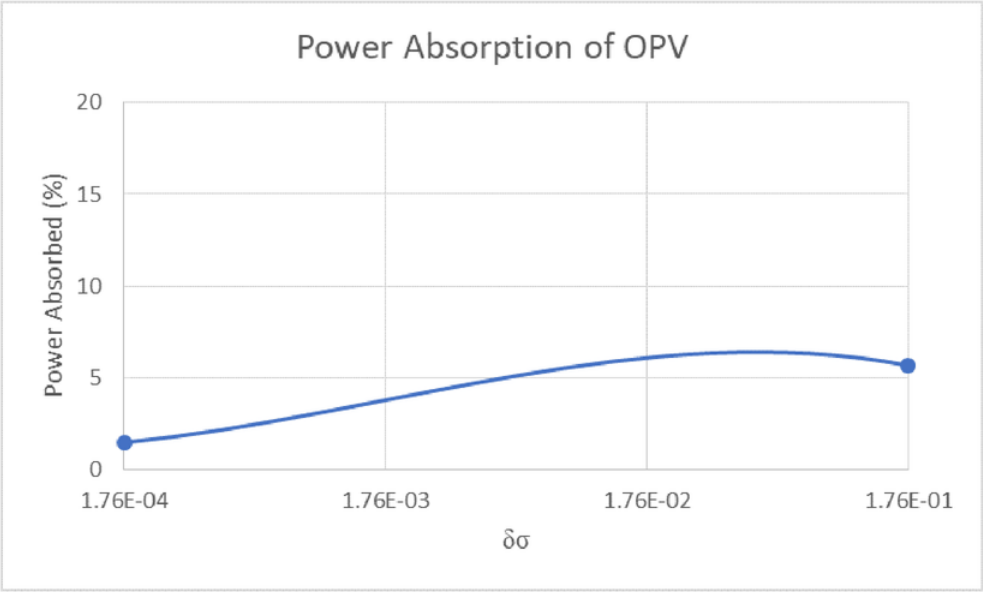

Figure 5.10: Power absorbed by OPV with different photoconductivity

5.2.2 Silicon

Silicon material simulated in this section has σ_{dark} of 0.312 $\frac{S}{m}$. This is the lowest conductivity Silicon material simulated in Chapter 4 and it has resonance frequency at 8.602 GHz. This frequency is fixed and the rest of the simulation is carried out by changing the conductivity of the material according to σ_{light} values as shown in table 5.4 and the power readings are obtained at this frequency. In chapter 4, silicon was losing its resonance at high conductivity, since this section uses silicon with even higher conductivity, open waveguide model discussed in chapter 3 was used rather than cavity model 1.

Material Specification

- Test sample placement (along z axis): 36mm
- Dielectric constant ($\frac{\epsilon_s}{\epsilon_0}$): 11.9
- Test Sample thickness: 1 μm
- Mobility: $\mu_n = 0.145\ m^2/Vs$ and $\mu_p = 0.05\ m^2/Vs$
- Conductivity (σ_{light}): Refer to Table 5.4

Table 5.4: Material conductivity of Silicon when light is flashed onto it

Doping (δn and δp) (m^{-3})	σ_{light} ($\frac{S}{m}$)
1×10^{22}	312
1×10^{25}	3.12×10^5
1×10^{28}	3.12×10^8

Field Distribution

Figure 5.11 displays the e-field distribution inside the cavity with silicon deposited on top of quartz. Input port for this waveguide is the port facing towards the viewer. Figure 5.11 (a) has the open waveguide with silicon's conductivity of 312 S/m, the figure clearly shows that most of the e-fields travel through the sample and reach port 2 (i.e. output port) and some are reflected. The maximum resulting amplitude of e-field is 3050 V/m and is towards the input side. In figure 5.11 (b), conductivity of the silicon is 3.12×10^5 S/m. Here, very small amount of e-fields can travel through the sample and towards the output port. There is very high power reflection which can be seen graphically and resulting amplitude is increased to 4674 V/m. In figure 5.11 (c), silicon is behaving like a metal blocking the power from reaching output port and in turn is reflecting all the power back to the input port. This has virtually turned the open waveguide into a closed waveguide by blocking the fields from travelling to port 2. Since input fields and reflected fields pass one and another, the resulting amplitude of these fields has increased to 4714 V/m.

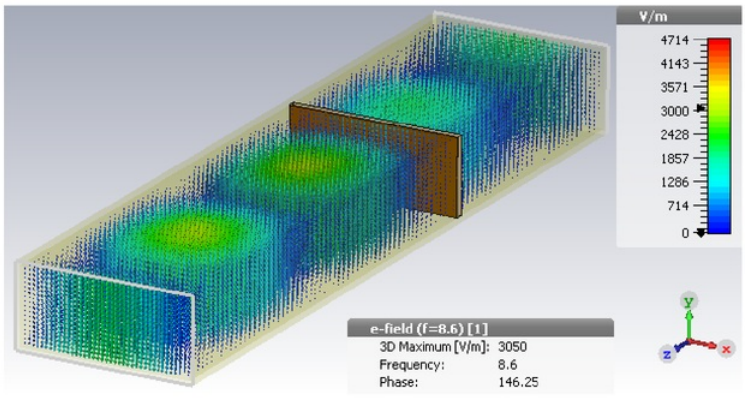

(a) Silicon with Conductivity of 312 $\frac{S}{m}$

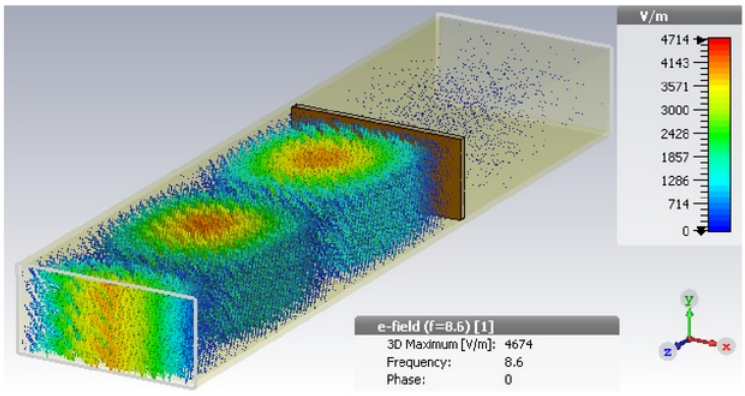

(b) Silicon Conductivity 3.12×10^5 $\frac{S}{m}$

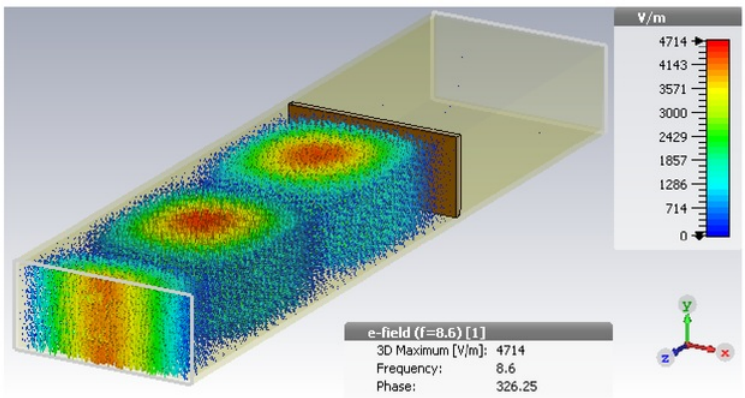

(c) Silicon Conductivity 3.12×10^8 $\frac{S}{m}$

Figure 5.11: E-Field distribution for Silicon with different photoconductivity

Power Analysis

The results discussed graphically previously by looking at the e-field in the waveguide is supported by the quantitative results shown in Figure 5.12 and 5.13. Silicon absorbs approximately 14% of power when $\delta\sigma$ is low. As $\delta\sigma$ is increased, silicon starts behaving like a metal or a mirror that reflects microwaves. At $\delta\sigma$ of 3.12×10^5 and higher, the power transmission from input port to output port is zero. The sensitivity factor, K, is approximately 6.7×10^{-7}.

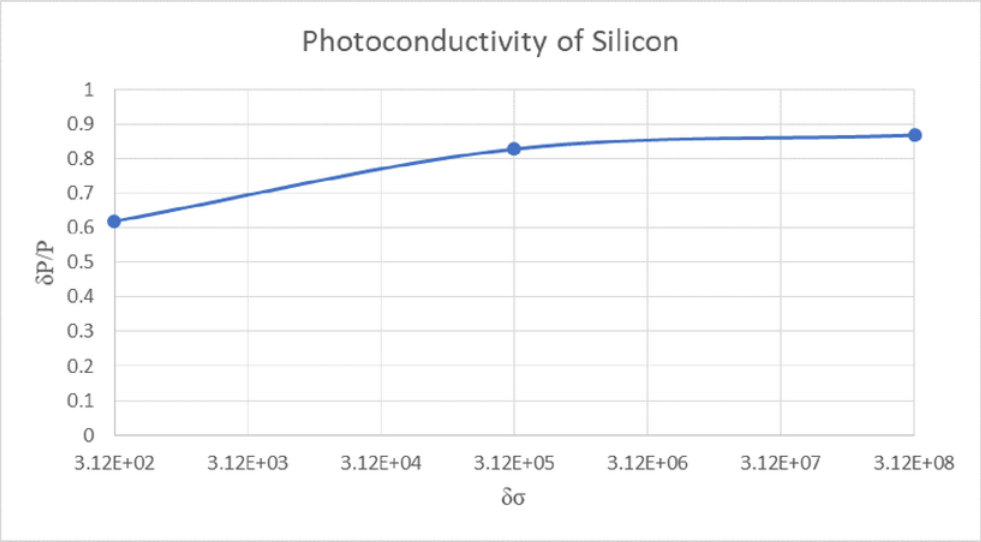

Figure 5.12: Power absorbed by Silicon with different photoconductivity

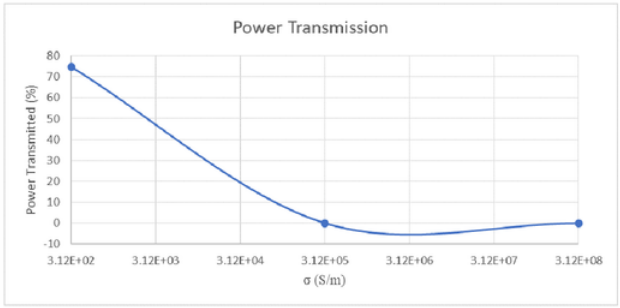

(a) Power Transmission in presence of Silicon

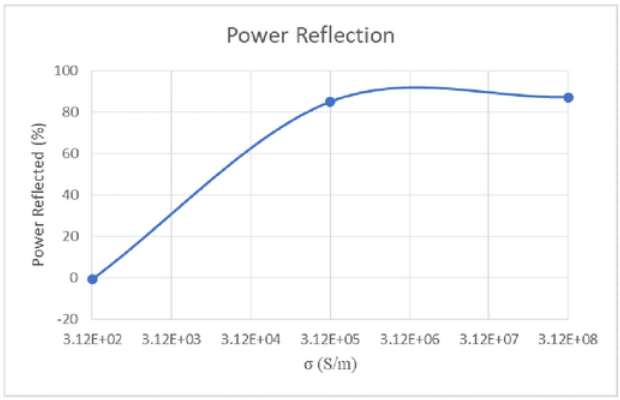

(b) Power Reflected by the Silicon

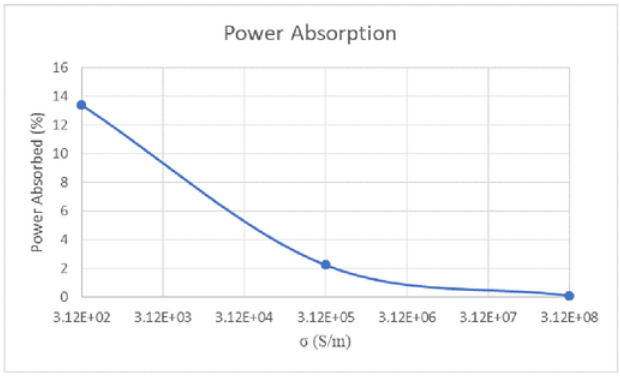

(c) Power Absorbed by the Silicon

Figure 5.13: Power graphs for silicon with different photoconductivity

5.2.3 Cadmium Telluride

Cadmium Telluride (CdTe) material simulated in this section has σ_{dark} of 0.184 $\frac{S}{m}$. This is the lowest conductivity CdTe material simulated in Chapter 4 and it has resonance frequency at 8.604 GHz. This frequency is fixed and the rest of the simulation is carried out by changing the conductivity of the material according to σ_{light} values as shown in table 5.5 and the power readings are obtained at this frequency. In chapter 4, CdTe was losing its resonance at high conductivity, since this section uses CdTe with even higher conductivity, open waveguide model discussed in chapter 3 was used rather than cavity model 1.

Material Specification

- Test sample placement (along z axis): 36mm
- Dielectric constant ($\frac{\epsilon_s}{\epsilon_0}$): 10.2
- Test Sample thickness: 1 μm
- Mobility: $\mu_n = 0.105\ m^2/Vs$ and $\mu_p = 0.01\ m^2/Vs$
- Conductivity (σ_{light}): Refer to Table 5.5

Table 5.5: Material conductivity of CdTe when light is flashed onto it

Doping (δn and δp) (m^{-3})	σ_{light} ($\frac{S}{m}$)
1×10^{22}	1.84×10^2
1×10^{25}	1.84×10^5
1×10^{28}	1.84×10^8

Field Distribution

Figure 5.14 displays the e-field distribution inside the cavity with CdTe deposited on top of quartz. Input port for this waveguide is the port facing towards the viewer. Figure 5.14 (a) has the open waveguide with CdTe's conductivity of 184 S/m, the figure clearly shows that most of the e-fields travel through the sample and reach port 2 (i.e. output port) and some are reflected. The maximum resulting amplitude of e-field is 3700 V/m and is towards the input side. In figure 5.14 (b), conductivity of the CdTe is 1.84×10^5 S/m. Here, very small amount of e-fields can travel through the sample and towards the output port. There is very high power reflection which can be seen graphically and resulting amplitude is increased to 4480 V/m. In figure 5.14 (c), CdTe is behaving like a metal blocking the power from reaching output port and in turn is reflecting all the power back to the input port. This has virtually turned the open waveguide into a closed waveguide by blocking the fields from travelling to port 2. Since input fields and reflected

fields pass one and another, the resulting amplitude of these fields has increased to 4527 V/m.

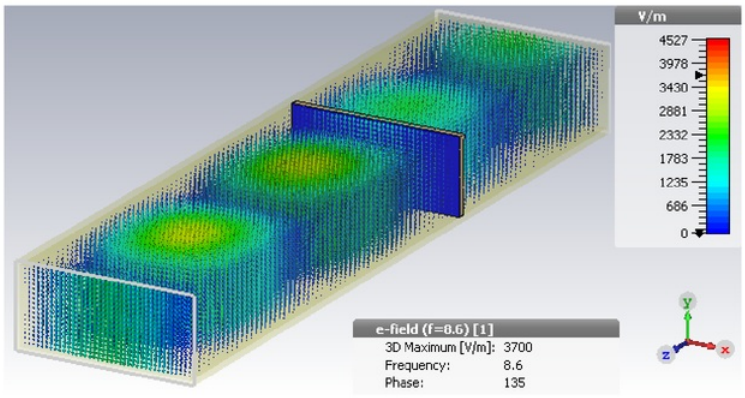

(a) CdTe with Conductivity of 184 $\frac{S}{m}$

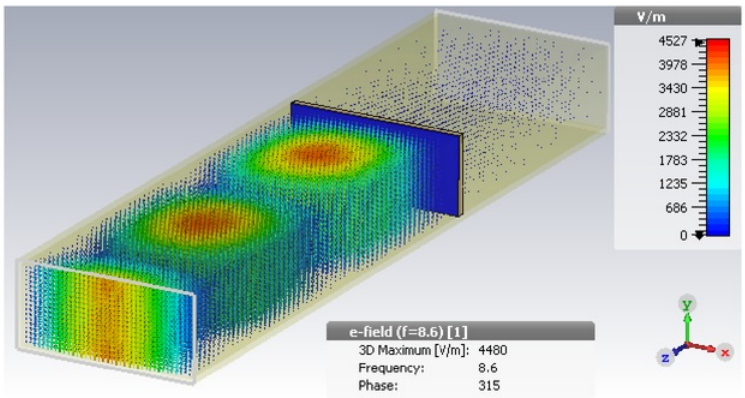

(b) CdTe Conductivity 1.84×10^5 $\frac{S}{m}$

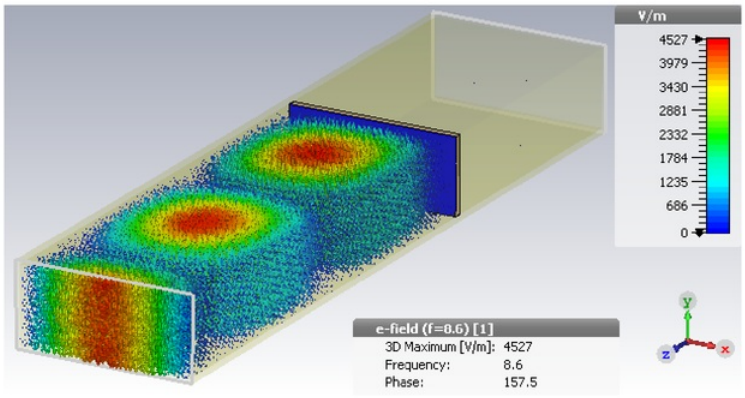

(c) CdTe Conductivity 1.84×10^8 $\frac{S}{m}$

Figure 5.14: E-Field distribution for CdTe with different photoconductivity

Power Analysis

The results discussed graphically previously by looking at the e-field in the waveguide is supported by the quantitative results shown in Figure 5.15 and 5.16. CdTe absorbs approximately 9% of power when $\delta\sigma$ is low. As $\delta\sigma$ is increased, CdTe starts behaving like a metal or a mirror that reflects microwaves. At $\delta\sigma$ of 1.84×10^5 and higher, the power transmission from input port to output port is zero. The sensitivity factor, K, is approximately 5.4×10^{-7}.

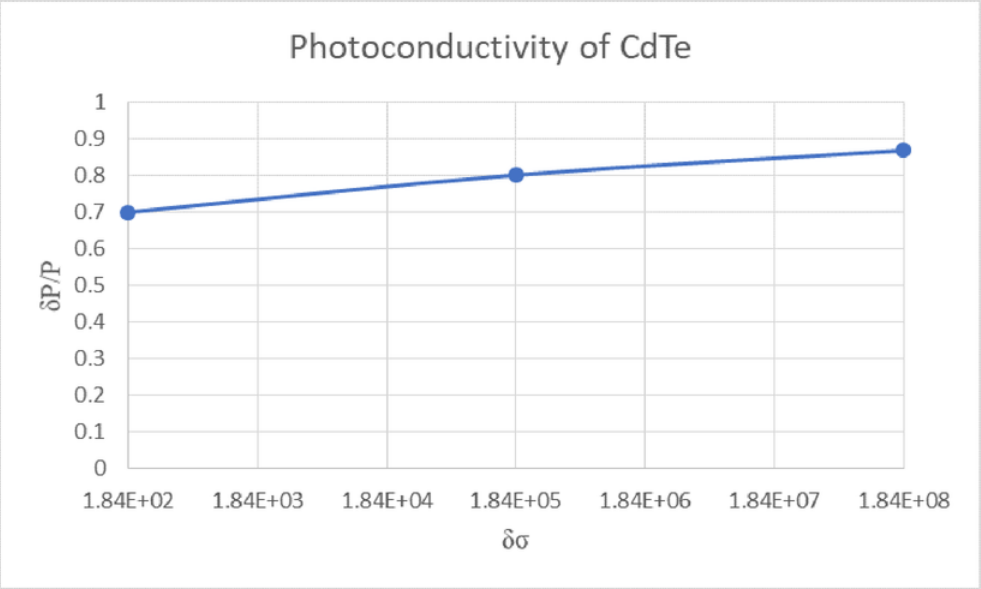

Figure 5.15: Power absorbed by CdTe with different photoconductivity

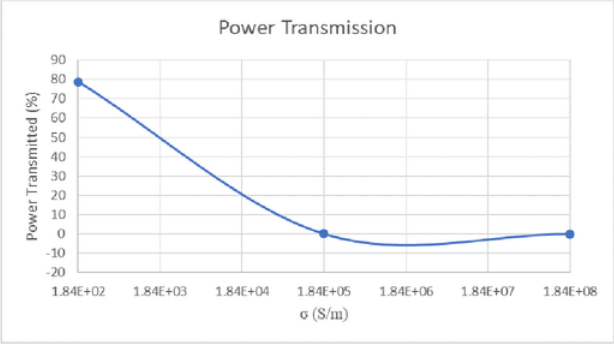

(a) Power Transmission in presence of CdTe

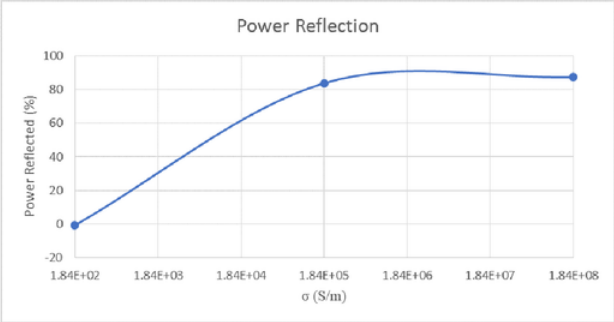

(b) Power Reflected by the CdTe

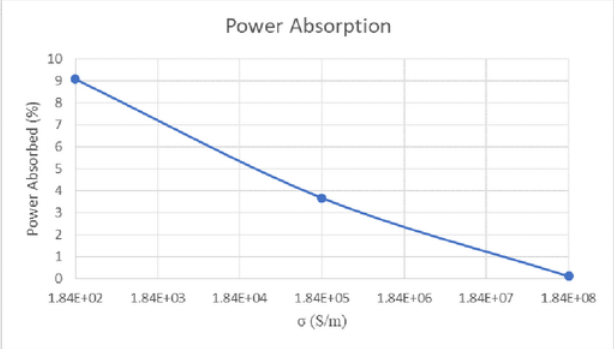

(c) Power Absorbed by the CdTe

Figure 5.16: Power graphs for CdTe with different photoconductivity

5.2.4 Gallium Arsenide

Gallium Arsenide (GaAs) material simulated in this section has σ_{dark} of 1.344 $\frac{S}{m}$. This is the lowest conductivity GaAs material simulated in Chapter 4 and it has resonance frequency at 8.6 GHz. This frequency is fixed and the rest of the simulation is carried out by changing the conductivity of the material according to σ_{light} values as shown in table 5.6 and the power readings are obtained at this frequency. In chapter 4, GaAs was losing its resonance at high conductivity, since this section uses GaAs with even higher conductivity, open waveguide model discussed in chapter 3 was used rather than cavity model 1.

Material Specification

- Test sample placement (along z axis): 36mm
- Dielectric constant ($\frac{\epsilon_s}{\epsilon_0}$): 12.9
- Test Sample thickness: 1 μm
- Mobility: $\mu_n = 0.8\ m^2/Vs$ and $\mu_p = 0.04\ m^2/Vs$
- Conductivity (σ_{light}): Refer to Table 5.6

Table 5.6: Material conductivity of GaAs when light is flashed onto it

Doping (δn and δp) (m^{-3})	σ_{light} ($\frac{S}{m}$)
1×10^{22}	1.34×10^3
1×10^{25}	1.34×10^6
1×10^{28}	1.34×10^9

Field Distribution

Figure 5.17 displays the e-field distribution inside the cavity with GaAs deposited on top of quartz. Input port for this waveguide is the port facing towards the viewer. Figure 5.17 (a) has the open waveguide with GaAs's conductivity of 1344 S/m, the figure clearly shows that some of the e-fields travel through the sample and reach port 2 (i.e. output port) and some are reflected. The maximum resulting amplitude of e-field is 3140 V/m and is towards the input side. In figure 5.17 (b), conductivity of the GaAs is 1.34×10^6 S/m. Here, barely any e-fields can travel through the sample and towards the output port. There is very high power reflection which can be seen graphically and resulting amplitude is increased to 4636 V/m. In figure 5.17 (c), GaAs is behaving like a metal blocking the power from reaching output port and in turn is reflecting all the power back to the input port. This has virtually turned the open waveguide into a closed waveguide by blocking the fields from travelling to port 2. Since input fields and reflected fields pass one and another, the resulting amplitude of these fields has increased to 4655 V/m.

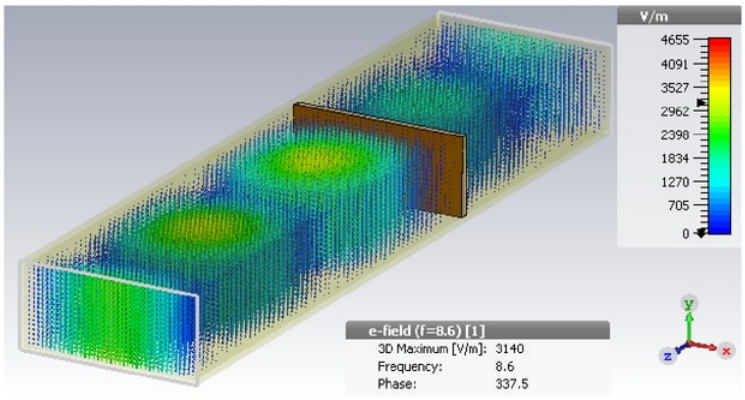

(a) GaAs with Conductivity of 1344 $\frac{S}{m}$

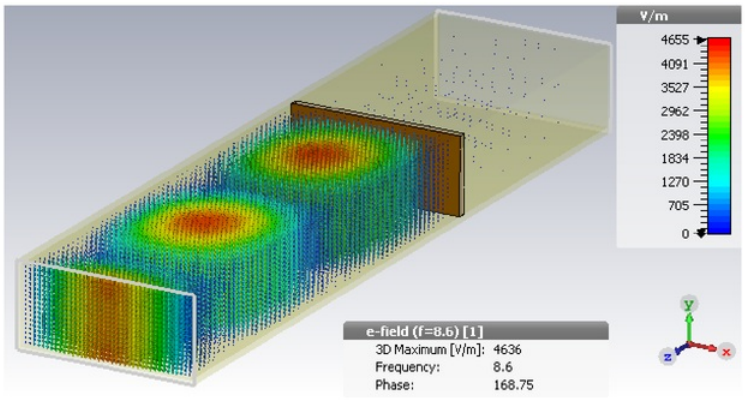

(b) GaAs Conductivity 1.34×10^6 $\frac{S}{m}$

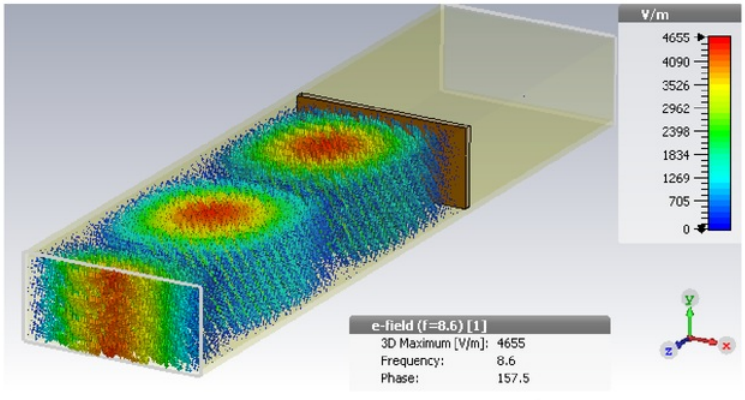

(c) GaAs Conductivity 1.34×10^9 $\frac{S}{m}$

Figure 5.17: E-Field distribution for GaAs with different photoconductivity

Power Analysis

The results discussed graphically previously by looking at the e-field in the waveguide is supported by the quantitative results shown in Figure 5.18 and 5.19. GaAs absorbs approximately 35% of power when $\delta\sigma$ is low. As $\delta\sigma$ is increased, GaAs starts behaving like a metal or a mirror that reflects microwaves. At $\delta\sigma$ of 1.34×10^6 and higher, the power transmission from input port to output port is zero. The sensitivity factor, K, is approximately 5.2×10^{-7}.

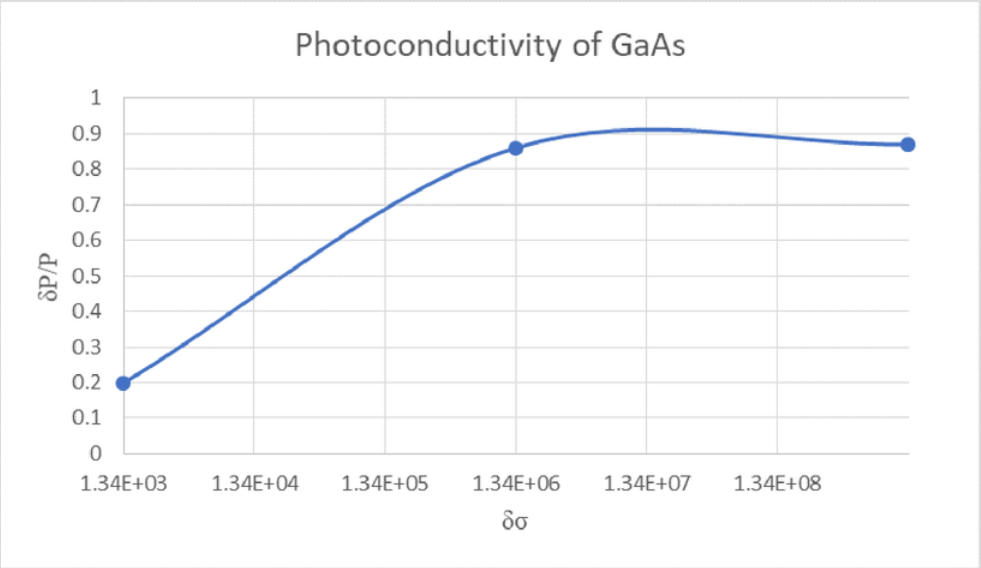

Figure 5.18: Power absorbed by GaAs with different photoconductivity

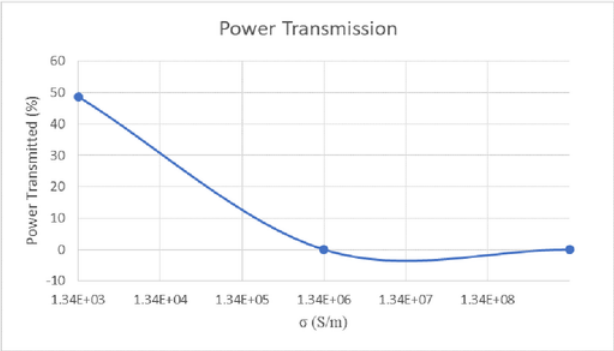

(a) Power Transmission in presence of GaAs

(b) Power Reflected by the GaAs

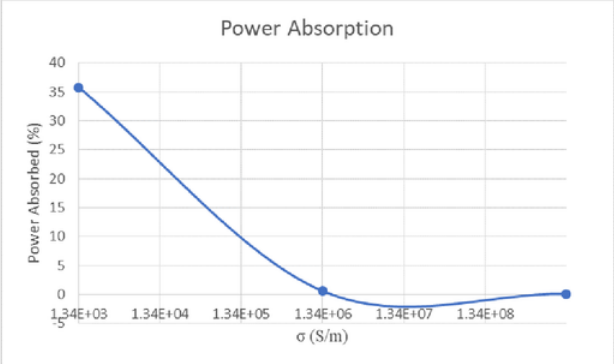

(c) Power Absorbed by the GaAs

Figure 5.19: Power graphs for GaAs with different photoconductivity

5.3 Conclusion

In this chapter sample materials and real PV materials were simulated to investigate the photoconductive aspects of these materials. Sample material 1, 2 and OPV were simulated using cavity model I whereas, Silicon, CdTe and GaAs were simulated using open waveguide model discussed in chapter 3. Sample material 1 had a higher material conductivity than sample material 2 when there is no light. Due to this fact, sample material 2 needed higher $\delta\sigma$ to match the power absorption of material 1. OPV can absorb maximum power of about 6% with high $\delta\sigma$. However, silicon has the capacity to absorb maximum power of 14%, CdTe can absorb 9% and GaAs can absorb maximum of 35% of the input power for low $\delta\sigma$. At high $\delta\sigma$, Silicon, CdTe and GaAs behave like metals which reflects the microwaves rather than absorbing. At doping of 10^{25} m^{-3}, Silicon, CdTe and GaAs have power reflections higher than 80% and OPV with 10^{28} m^{-3} doping has high power reflection and these are the major contributors in disrupting the waveguide and cavity measurements. This indicates the limitations of the proposed model.

Chapter 6

Summary and Future Work

This thesis looked at the feasibility of an alternative microwave system for measuring dark and photoconductivity of semiconductors. Different configurations of open waveguide and cavity was modelled and simulated using CST. Samples were tested in open waveguide and in cavity resonator. Cavity resonator was designed from rectangular waveguide from which the rest of the simulations of semiconductor materials were carried out. After understanding the semiconductor material's interaction with microwaves, these material are excited virtually by the light flash. This excitation was modelled by changing the conductivity of the material. Real photovoltaic materials were modelled and simulated in cavity and open waveguide.

One of the motivations was to investigate if this design can be used to test not just low conductivity sample but also high conductivity samples. After analysing the results obtained in this thesis, the proposed design works very well for samples with low conductivity such as OPV, however for silicon, GaAs and CdTe, the design needs to be modified. When probing for photoconductivity in samples with high dark conductivity, the samples were shorting the cavity. So these samples were simulated using open waveguide configuration. Cavity design worked really well while probing dark and photoconductivity in OPV samples.

The other motivation was to get good qualitative results in particular, field maps of the interaction between E-fields and different samples, which could support the mathematical analysis. The simulation results show the e-field interaction with samples and also quantitatively indicates how the amplitude of e-field varies depending on the surroundings (i.e. model and sample material). This gives a clear visualisation of when and how the fields behave when there is good cavity and when the model is losing its cavity. These results supported the mathematical results in particular, the quality of the cavity and the resonance curves. Overall, these observations indicate that the proposed design is suitable for probing low conductivity semiconductor materials and for high conductivity the design needs to be modified.

Based on the results obtained in this thesis and the conclusions, this thesis can be continued in many directions in future. For instance, since this thesis looked at just four real PV materials, in future more semiconductor materials with wide range of conduc-

tivities can be explored. Different geometries of model can be explored by changing the position and orientation of the sample within the waveguide and cavity. Different shapes of waveguides and cavities can be used to see its effect on the microwave absorption by the sample.

Chapter 7

Abbreviations

TRMC	Time Resolved Microwave Conductivity
FP-TRMC	Flash Photolysis Time Resolved Microwave Conductivity
CST	Computer simulation technology
TE	Transverse Electric mode
TM	Transverse Magnetic mode
EM waves	Electromagnetic waves
E-field	Electric field
H-field	Magnetic field
RL	Return loss
IL	Insertion loss
P_I	Input Power
P_R	Reflected Power
P_T	Transmitted Power
P_A	Absorbed Power
σ_{dark}	Conductivity of the material when there is no light
σ_{light}	Conductivity of the material when there is light
$\delta\sigma$	Photoconductivity
$\delta P/P$	Normalised power
Q_L	Quality of the cavity
K	Sensitivity factor

Appendix A

Consultation form and Project Plan

A.1 Consultation Meetings Attendance Form

Consultation Meetings Attendance Form

Week	Date	Comments (if applicable)	Student's Signature	Supervisor's Signature
1	3/8/17	Discussing and planning initial stages of proj.	Rakshita.R	NG.
2	8/8/17	Project progress & first calculations	Rakshita.R	NG.
3	14/8/17	Project progress & data processing	Rakshita.R	NG.
5	31/8/17	Project progressing nicely, first results.	Rakshita.R	NG
6	5/9/17	Good progress, real sample simulations	Rakshita.R	NG
7	12/9/17	All well, simulations progressing to last stage	Rakshita.R	NG
Sem. break.	28/9/17	Cavity simulations using full version	Rakshita.R	NG
8	6/10/17	Case studies of real PV samples	Rakshita.R	NG.
11	25/10/17	Progress Report Feedback	Rakshita.R	NG
12	3/11/17	Thesis Report Feedback	Rakshita.R	NG.

Figure A.1: Consultation Form

A.2 Thesis Timeline

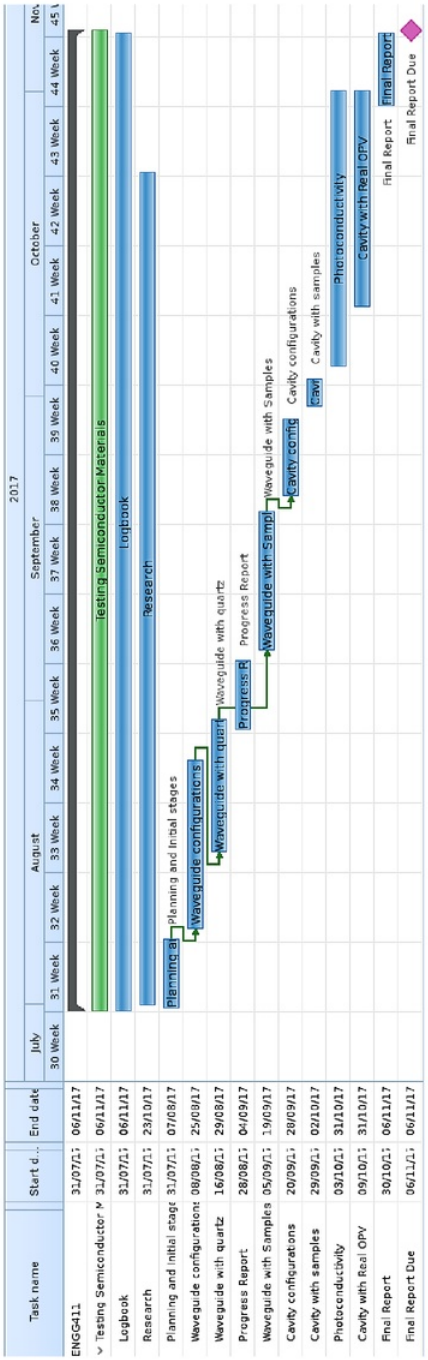

Figure A.2: Gantt Chart

Bibliography

[1] R. Paschotta. Pump-probe measurements. [Online]. Available: https://www.rp-photonics.com/pump_probe_measurements.html

[2] NREL. Probing solar photo conversion using flashphotolysis timeresolved microwave conductivity. [Online]. Available: https://energysciences.nrel.gov/sites/default/files/embedded/files/fp_trmc_training_1.pdf

[3] O. Ostroverkhova, *Handbook of Organic Materials for Optical and (Opto)Electronic Devices*, 1st ed. Woodhead Publishing, 2013.

[4] J. E. Kroeze, *Photoinduced Charge Separation In Dye-Sensitized Films Of Smooth and Nanocrystalline Tio2*. The Netherlands: DUP Science, 2004.

[5] N. R. Council, *Microwave Processing of Materials*. Washington, DC: The National Academies Press, 1994.

[6] J. J. Carr, *Practical Antenna Handbook*, 4th ed. McGraw-Hill, 2001.

[7] C. Studio. Waveguides - rectangular waveguides. [Online]. Available: https://www.cst.com/academia/examples/hollow-rectangular-waveguide

[8] R. WIreless. Vector network analyzer tutorial — vna tutorial. [Online]. Available: http://www.rfwireless-world.com/Tutorials/Vector-Network-Analyzer-VNA-tutorial.html

[9] Y. Fujishiro. Taking advantage of s-parameter. [Online]. Available: https://product.tdk.com/en/products/emc/guidebook/eemc_basic_03.pdf

[10] D. M. Pozar, *Microwave Engineering*, 3rd ed. John Wiley, 2005.

[11] T. Bird, "Definition and Misuse of Return Loss, journal =."

[12] M. Hyde. What is the difference between returnloss(db) and s11(db). [Online]. Available: https://www.researchgate.net/post/What_is_the_difference_between_ReturnlossdB_and_S11dB

[13] C. Studio. Cst micorwave studio — transient solver. [Online]. Available: https://www.cst.com/products/cstmws/solvers/transientsolver